

ELUCIDATING THE DESIGN SPACE OF FP4 TRAINING

Robert Hu & Carlo Luschi & Paul Balanca

Graphcore

London, UK

{roberthu, carlo, paulb}@graphcore.ai

ABSTRACT

The increasing computational demands of foundation models have spurred research into low-precision training, with 4-bit floating-point (FP4) formats emerging as a frontier for maximizing hardware throughput. While numerous techniques have been proposed to stabilize FP4 training, they often present isolated solutions with varying, and not always clear, computational overheads. This paper aims to provide a unified view of the design space of FP4 training. We introduce a comprehensive, quantisation gradient-based framework for microscaling quantization that allows for a theoretical analysis of the computational costs associated with different stabilization methods on both the forward and backward passes. Using a simulator built on this framework, we conduct an extensive empirical study across a wide range of machine learning tasks, including regression, image classification, diffusion models, and language models. By systematically evaluating thousands of combinations of techniques—such as novel gradient approximations, rounding strategies, and scaling methods, we identify which configurations offer the most favourable performance-to-overhead trade-off. We find that the techniques enabling the best trade-off involve carefully combining Hadamard transformations, tensor scaling and stochastic rounding. We further find that using UE5M3 as a scaling factor potentially offers a good compromise between range and precision with manageable computational overhead.

1 INTRODUCTION

With the emergence of foundation models (Bommasani et al., 2021), the demand for computational resources has grown proportionally to the parameter count of these models, which often span from billions to trillions of parameters. Many of these models rely on the transformer architecture (Vaswani et al., 2017), which is ubiquitous across vision, text and video models (Khan et al., 2022). These models tend to be compute bound by two operations: the attention mechanism (Duman-Keles et al., 2023; Dolga et al., 2024) which tends to scale quadratically with sequence length, and the matmul operations from the weight matrices (Corp, 2025) which are quadratic with respect to size of the hidden dimensions.

In this paper, we conduct the first large-scale, systematic investigation of the FP4 design space. Traditionally, machine learning training uses FP32 format which serves as the baseline with the highest accuracy and lowest throughput. Historically, with each subsequent generation of hardware, the precision has been halved — starting from 2016 FP16 (Micikevicius et al., 2018), 2022 FP8 (Noune et al., 2022; Micikevicius et al., 2022; Fishman et al., 2025), and now 2025 with FP4 (Chmiel et al., 2025; Castro et al., 2025). Halving the precision often allows a doubling of the throughput for matrix multiplication operations (Hao et al., 2025), hence with each iteration careful adjustments need to be made to the training procedure to account for the loss of numerical accuracy (Tseng et al., 2024; Li et al., 2025). There have been several previous works accounting for FP16 (Micikevicius et al., 2018), FP8 (Fishman et al., 2025), and recently FP4 (Tseng et al., 2025; Chen et al., 2025; Castro et al., 2025; Hao et al., 2025; Chmiel et al., 2025; Wang et al., 2025; Yang et al., 2025; Su et al., 2025; Li et al., 2025; Cao et al., 2025).

While these works introduce new techniques to stabilize FP4 training for larger models, they all propose different methodologies with varying computational overhead that are empirically shown to work in isolation through simulations in BFLOAT16. However, a systematic evaluation of the

performance-overhead trade-offs has been missing. As an example, Wang et al. (2025) introduces a quantile based pruning and gradient adjustment, both of which are shown to be useful, however both add an additional $\sim \mathcal{O}(n)$ time and memory overhead which cannot be done in low-precision and is non-fusable. It should be further noted that the simulation procedure in Wang et al. (2025) does not adequately quantise the scale, which their description implies is kept in high-precision – a detail that can significantly impact training stability. Similarly, Tseng et al. (2025) proposes a block-wise Hadamard transformation, which induces a $\sim \mathcal{O}(n \log l)$ overhead. It should be noted that none of the aforementioned papers simulate FP 4 training fully, as Wang et al. (2025) only consider quantising weights and activations and not the gradient and Tseng et al. (2025) only quantises the gradient. Further, Cao et al. (2025); Li et al. (2025) proposes spectral decomposition techniques to handle outliers, which consequently introduces $\mathcal{O}(mnk)$ time and $\mathcal{O}(k^2)$ memory, which in terms of hardware acceleration is also non-fusable. It is currently not clear whether these additional overheads are necessary in downstream implementations of low-precision matrix multiplication, as some evidence in Chmiel et al. (2025); Yang et al. (2025) suggests that something as simple as *Stochastic Rounding (SR)* is enough to stabilise FP 4 training.

The goal of this work is to develop a thorough understanding of the quantisation mechanism and how it affects the training procedure and illuminate which techniques offer a worthwhile trade-off in terms of additional overhead vs performance benefit. We summarise the contributions of this paper as follows:

1. We propose a quantisation gradient-based framework for FP 4 quantisation, which is used to derive the computational overhead of conceivably useful techniques (both novel and existing ones) on the forward and backward pass of a quantised linear layer.
2. We implement the framework as a simulator, running experiments of across various machine learning tasks to gain insight on which combination of techniques offer a reasonable overhead vs. performance benefit.

We first introduce our unified, gradient-based framework in Section 2, then use it to analyze the design space of scaling, rounding, and gradient approximation techniques in Sections 3, 4, and 5. We survey other relevant methods in Section 6, present our extensive empirical validation in Section 7, and conclude with our key findings.

2 A COMMON FRAMEWORK FOR FP 4 TRAINING

In this section, we detail what happens when we use microscaling formats to quantize a tensor for a linear layer forward pass. Consider a tensor $\mathbf{X} \in \mathbb{R}^{m \times n}$. We first define \mathbf{X} represented in microscaling format Rouhani et al. (2023).

Definition 1. A micro-scaled block is defined by a scalar $s \in \mathbb{R}$ and a vector $\mathbf{P} = [p_i]_{i=1}^l$ of l elements. Each value x_i can be recovered as

$$x_i = s \cdot p_i.$$

The parameter l is a fixed constant known as the block size. Given a tensor $\mathbf{X} \in \mathbb{R}^{m \times n}$ and a block size of l , the MX representation of \mathbf{X} consists of a collection of tuples

$$\{(s_j, \mathbf{P}_j)\}_{j=1}^{(m \cdot n)/l},$$

where each tuple corresponds to a block of l elements in \mathbf{X} .

Intuitively, microformat scaling represents partitions of a tensor with a common scale often used to normalise the partition, where the scaled elements \mathbf{P}_j is quantized to a lower precision. We formally detail the quantisation procedure for one partition $\mathbf{X}_p \in \mathbb{R}^l$ below, represented by a transformation f :

$$f(\mathbf{X}_p) = \frac{1}{s_q} Q(s_q \cdot \mathbf{X}_p)$$

where the components are defined as follows:

Outer Scaling Factor (s_q): This factor is a function of \mathbf{X}_p . First, an intermediate factor $s(\mathbf{X}_p)$ is computed:

$$s(\mathbf{X}_p) = \frac{\text{FP 4 max}}{Z(\mathbf{X}_p)}$$

Here, $Z : \mathbb{R}^l \rightarrow \mathbb{R}$ is a scalar-valued function of the tensor \mathbf{X}_p (e.g., the absolute maximum norm, `absmax`). This factor is then quantized:

$$s_q = q(s(\mathbf{X}_p))$$

Quantization Function (Q): Q is an element-wise function that quantizes the elements of \mathbf{X}_p .

We can now introduce the gradient with respect to an element in \mathbf{X} :

Proposition 1. *Let $f(\mathbf{X}_p) = \frac{1}{s_q} Q(s_q \cdot \mathbf{X}_p)$ Then, the partial derivative of f_{ij} with respect to \mathbf{X}_{ij} is given by:*

$$\boxed{\frac{\partial f_{ij}}{\partial \mathbf{X}_{ij}} = Q'(s_q \mathbf{X}_{ij}) + \frac{\partial s}{\partial \mathbf{X}_{ij}} \left[\frac{q'(s)}{s_q} \left(\mathbf{X}_{ij} Q'(s_q \mathbf{X}_{ij}) - \frac{1}{s_q} Q(s_q \mathbf{X}_{ij}) \right) \right]} \quad (1)$$

See Section .7 for derivations.

In the context of a linear layer with weights $\mathbf{W} \in \mathbb{R}^{n \times m}$ and input data $\mathbf{X} \in \mathbb{R}^{b \times m}$, the output $\mathbf{Y} = f(\mathbf{X})f(\mathbf{W})^\top$ would have the corresponding gradients:

$$\frac{\partial \mathcal{L}}{\partial \mathbf{X}} = \left(\frac{\partial \mathcal{L}}{\partial \mathbf{Y}} \cdot f(\mathbf{W}) \right) \odot \frac{\partial f(\mathbf{X})}{\partial \mathbf{X}}, \quad \frac{\partial \mathcal{L}}{\partial \mathbf{W}} = \left(\left(\frac{\partial \mathcal{L}}{\partial \mathbf{Y}} \right)^\top \cdot f(\mathbf{X}) \right) \odot \frac{\partial f(\mathbf{W})}{\partial \mathbf{W}}.$$

Here, \mathcal{L} denotes the scalar loss, \odot the elementwise product and $f(\cdot)$ is a differentiable transformation (e.g., MX decomposition or quantization-aware mapping) applied to the inputs and weights. In the next section, we detail different choices in terms of calculating and approximating $\frac{\partial \mathcal{L}}{\partial \mathbf{X}}, \frac{\partial \mathcal{L}}{\partial \mathbf{W}}$. We summarise the time and memory overhead of our proposed and existing techniques in Table 2.

3 TENSOR SCALING IN FP 4 TRAINING

An alternative to applying block-wise scaling directly is to first normalize the entire tensor Blake et al. (2023); Micikevicius et al. (2022); Sun et al. (2019); Peng et al. (2023). The goal of this strategy is to improve the quantization of the scaling factors themselves. In this approach, a tensor-wise scaling factor g is computed, used to normalize the tensor, and then multiplied back after the block-wise quantization. While the intent is for g to cancel out, the non-linear nature of the scale quantization function $q(\cdot)$ results in a distinct final transformation.

Let $g = \max_p \{m_p\}$, $m_p = Z(\mathbf{X}_p)$ be the global scaling factor for a tensor \mathbf{X} , and let $\mathbf{U} = \mathbf{X}/g$ be the globally normalized tensor. The transformation $h(\mathbf{X})$ for an element \mathbf{X}_{ij} within a block p is defined as $h_{ij}(\mathbf{X}_p) = g \cdot f_{ij}(\mathbf{U}_p)$.

Here, $f(\mathbf{U}_p)$ is the block-wise quantization function from Section 2 applied to the normalized block \mathbf{U}_p . Its components are functions of \mathbf{U}_p :

1. **Ideal Scale:** $s'_p = \frac{\text{FP 4}_{\max}}{Z(\mathbf{U}_p)} = g \cdot \frac{\text{FP 4}_{\max}}{Z(\mathbf{X}_p)} = g \cdot s_p$
2. **Quantized Scale:** $s'_{q,p} = q(s'_p) = q(g \cdot s_p)$

Substituting these gives the full forward pass expression for an element:

$$\boxed{h_{ij}(\mathbf{X}) = \frac{g}{q(g \cdot s_p)} Q \left(q(g \cdot s_p) \cdot \frac{\mathbf{X}_{ij}}{g} \right)} \quad (2)$$

The gradient of this transformation accounts for both the block-wise dependencies and the global dependency on g .

Corollary 1. *Let $h(\mathbf{X})$ be the quantization with intermediate global normalization. For an element \mathbf{X}_{ij} in block p , the partial derivative is:*

$$\boxed{\frac{\partial h_{ij}}{\partial \mathbf{X}_{ij}} = \frac{\partial f_{ij}}{\partial \mathbf{U}_{p,ij}} + \frac{\partial g}{\partial \mathbf{X}_{ij}} \left(f_{ij}(\mathbf{U}_p) - \mathbf{U}_{p,ij} \frac{\partial f_{ij}}{\partial \mathbf{U}_{p,ij}} \right)} \quad (3)$$

where $\frac{\partial f_{ij}}{\partial \mathbf{U}_{p,ij}}$ is the full gradient from the first Theorem, evaluated on the normalized block \mathbf{U}_p with its corresponding scales $(s'_p, s'_{q,p}, k'_p)$. See Section .8 for derivations.

It should be noted that g in context of the MXFP4 (FP4 format with E8M0 scale) and NVFP4 (FP4 format with E4M3 scale) has overhead complexity $\mathcal{O}((m \cdot n) // l)$ as opposed to $\mathcal{O}(m \cdot n)$ when computing $\text{absmax}(\mathbf{X})$, since it suffices to search the scales rather than the entire tensor \mathbf{X} .

3.1 ROUNDING AND SCALING STRATEGIES

Recent work in low-precision training has highlighted that the rounding strategy for scaling factors can have a profound impact on model stability. For instance, Mishra et al. (2025) found that for MXFP8 formats, rounding-to-positive-infinity improves signal propagation by reducing the number of saturated values, given the limited range of the scaling factor. As our work considers both E4M3 (which has a limited range) and E8M0 (which has a wider range), we evaluate both round-to-nearest (RTN) and round-to-positive-infinity in our experiments.

We note that the results in Chmiel et al. (2025) get NVFP4 to converge without any issues with tensor scaling, as they mitigate any overflow by taking $\tilde{s}_p = \frac{s'_p}{\text{FP4}_{\max} \cdot \text{E4M3}_{\max} \cdot 0.5}$. This pushes down the effective range of $\tilde{s}_p \in [2/\text{E4M3}_{\max}, 2/\text{E4M3}_{\max} \cdot g]$. While not completely protected from overflow, it's a good rule of thumb to maximize the utilised range of E4M3. We use this technique when applying tensor scaling for NVFP4. We note that this heuristic can be extended to any scale format beyond E4M3, as it effectively rescales the scale factor to utilise its maximum range.

Handling Zero-Valued Scales. A critical edge case is the handling of zero-valued scaling factors, resulting in division by zero in the dequantisation. Chmiel et al. (2025) replaces any zero scale with one, which may induce further quantisation errors as small scales are set to 1. We propose rounding the zeros and underflows to the closest representable subnormal value in the target format and saturate overflows to the maximum representable number. We compare the efficacy of both approaches in our experiments.

Rounding of the weight tensor The impact of the rounding strategy has previously been demonstrated in Chmiel et al. (2025); Fitzgibbon & Felix (2025) to have significant impact on the stability of LLM training in low-precision format. The main observations for FP4 formats is to use *round-to-nearest* (RTN) for the forward pass and *stochastic rounding* (SR) in backwards pass (Chmiel et al., 2025; Yang et al., 2025), specifically on the activation and gradient tensors. We follow the quantisation procedure in Rouhani et al. (2023), which considers 6 quantisations for a forward and backward pass in a linear layer. We benchmark against the proposed strategy in Chmiel et al. (2025) and additionally consider SR on the activations in the forward pass as well.

Rounding of the scales We also experiment with stochastic rounding in the scaling factor as well. We motivate this design choice with the observation that E8M0 has very large intervals between each number, leading to potential bias, which can be mitigated more effectively at the scaling factor.

4 DIFFERENTIABLE RELAXATIONS FOR QUANTIZATION

Approximating $Q'(\mathbf{X})$ and $q'(x)$ In Wang et al. (2025), they take $\frac{\partial f_{ij}}{\partial \mathbf{W}_{ij}} \approx Q'(s \cdot \mathbf{W}_{ij})$. However since Q is a quantisation function which is not differentiable, they approximate $Q(x) \approx \frac{\delta}{2} \cdot \left(1 + \text{sign}\left(\frac{2x}{\delta} - 1\right) \cdot \left|\frac{2x}{\delta} - 1\right|^{\frac{1}{w}}\right)$, with gradient $Q'(x) = \frac{1}{w} \cdot \left|\frac{2x}{\delta} - 1\right|^{\frac{1}{w}-1}$. They propose $w = 5$ in their implementation. There are some potential flaws with the proposed parametrisation, as calculating power of fractionals tends to be computationally expensive and require $\mathcal{O}(w)$ cycles. This leads to the overall complexity of $\mathcal{O}(nmw \log_2(k))$, where $\log_2(k)$ comes from finding the interval x belongs to on the E2M1 grid using binary search, with k being the grid size. We thus propose an alternative differentiable relaxation to $Q(x)$.

Linear Spline approximation A linear spline is a continuous piecewise linear function defined over a set of sorted knots t_0, \dots, t_n . These knots partition the domain into n intervals $I_i = [t_i, t_{i+1})$. The function's continuity is ensured by having the linear segments connect at the knots.

The forward and backward passes evaluate the spline and its derivative. For an input $x \in [t_i, t_{i+1})$, the spline is a line segment, $S(x) = a_i(x - t_i) + b_i$ (**Forward pass**) with $S'(x) = a_i$ (**Backward pass**). Here, b_i represents the value of the spline at knot t_i (i.e., $S(t_i)$), and a_i is the slope of the line segment over the interval $[t_i, t_{i+1})$.

We illustrate our proposed differentiable quantization approximation and its corresponding gradient in Fig. 1. The function is shown in Fig. 1a, and its gradient is depicted in Fig. 1b. We found that applying the quantisation gradient in the backwards pass sometimes would mask out the gradient entirely, hence we propose clipping $Q'(x)$ from below to prevent multiplying the gradient with 0 (Figure 1c). The overall complexity overhead of the spline approximation is thus $\mathcal{O}(nm \log_2(k))$.

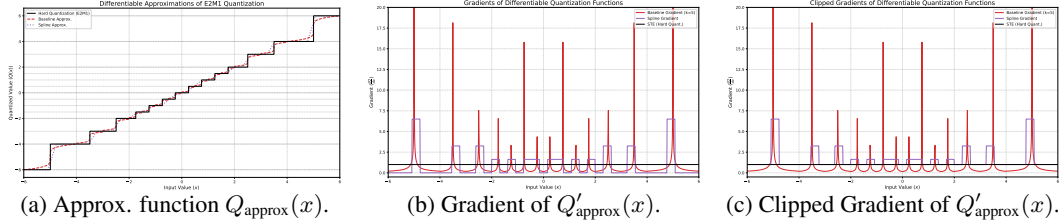


Figure 1: Approximations of $Q(x)$ and their corresponding gradients, assuming ties-to-even rounding. We refer to Wang et al. (2025) as the baseline.

Note that we need to save the unquantised matrix \mathbf{X} for the backwards pass to evaluate $Q'(\mathbf{X})$, adding $\mathcal{O}(mn)$ memory overhead.

5 GRADIENT ADJUSTMENT FOR SCALING FACTOR QUANTIZATION

The gradient adjustment techniques used for weights and activations can also be applied to the quantization of the scaling factor $q(s)$. However, the relatively high dynamic range required for scaling factors introduces additional complexity. To find a decent trade-off between accuracy and complexity, we first analyze the regions where the quantization error is most significant. We measure this error using the relative deviation, defined as the ratio s/s_q . A value of this ratio far from 1 indicates a large quantization error.

Figure 2 illustrates the quantization functions for the E4M3 and E8M0 scale formats and their corresponding relative deviations. The quantization function itself is shown in Fig. 2a, while the error is plotted in Fig. 2b.

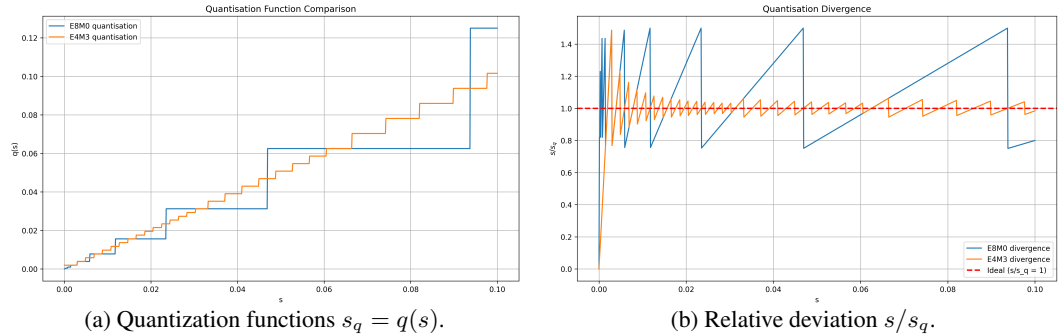


Figure 2: Comparison of quantization for E4M3 and E8M0 scaling factors. Figure (a) shows the quantization step functions. Figure (b) shows the relative deviation, which is most pronounced for small values of the scaling factor s .

As illustrated in Fig. 2b, the largest relative deviation occurs for small-magnitude scaling factors, especially within the first few representable values of the E4M3 scale format. Based on this observation, we can choose to apply the gradient adjustment selectively, targeting only the range where the quantization error is highest when computing the $q'(s)$ term.

5.1 GRADIENT ADJUSTMENT OF ABSMAX: ADJUSTING FOR $Z(\mathbf{X}_p)$ AND $s'(\mathbf{X}_p)$

First, we establish the general relationship between the gradient of the scaling factor, $\frac{\partial s}{\partial \mathbf{X}}$, and the gradient of the normalization function, $\frac{\partial Z}{\partial \mathbf{X}}$.

Proposition 2. Given the scaling factor $s(\mathbf{X}) = \frac{\text{FP4 max}}{Z(\mathbf{X})}$, its element-wise gradient with respect to an element \mathbf{X}_{ij} is given by:

$$\frac{\partial s}{\partial \mathbf{X}_{ij}} = -\frac{\text{FP4 max}}{Z(\mathbf{X})^2} \frac{\partial Z}{\partial \mathbf{X}_{ij}}$$

See Section .9 for derivations.

The following corollaries provide the specific form of this gradient for two common choices of the normalization function $Z(\mathbf{X})$.

Corollary 2. If the normalization function $Z(\mathbf{X})$ is *absmax*, $Z(\mathbf{X}) = \max_{k,l} |\mathbf{X}_{kl}|$, then the gradient of the scaling factor is non-zero only for the element with the maximum absolute value:

$$\frac{\partial s}{\partial \mathbf{X}_{ij}} = -\frac{\text{FP4 max}}{Z(\mathbf{X})^2} (\text{sign}(\mathbf{X}_{i^*j^*}) \cdot \delta_{ii^*} \delta_{jj^*}) \quad (4)$$

where (i^*, j^*) is the index of the maximum absolute value element and δ is the Kronecker delta. See Section .10 for derivations.

Corollary 3. If the normalization function $Z(\mathbf{X})$ is the smooth LogSumExp approximation of the max function, $Z(\mathbf{X}) = \frac{1}{\beta} \log \left(\sum_{k,l} e^{\beta |\mathbf{X}_{kl}|} \right)$, the gradient of the scaling factor is a dense gradient given by:

$$\frac{\partial s}{\partial \mathbf{X}_{ij}} = -\frac{\text{FP4 max}}{Z(\mathbf{X})^2} (\text{softmax}(\beta |\mathbf{X}|)_{ij} \cdot \text{sign}(\mathbf{X}_{ij})) \quad (5)$$

See Section .11 for derivations.

We consider four configurations for calculating the gradients with respect to the scaling factors, summarized in Table 1. Alongside the standard ‘Absmax’ and ‘Softmax’ approaches, we introduce a ‘Hybrid’ method. This approach uses the computationally efficient ‘absmax’ function in the forward pass but approximates its gradient with the dense ‘softmax’ derivative during the backward pass. This is intended to propagate gradient information to more elements without incurring the forward-pass cost of the LogSumExp operation.

Table 1: Gradient configurations for the block-wise scale $s(\mathbf{X})$ and global scale $g(\mathbf{X})$. The Straight-Through Estimator (STE) gradient is a heuristic approximation, as detailed in the text.

Configuration	Scaling Function $Z(\mathbf{X})$	Gradient $\frac{\partial s}{\partial \mathbf{X}_{ij}}$	Global Function $g(\mathbf{X})$	Scaling Gradient $\frac{\partial g}{\partial \mathbf{X}_{ij}}$
STE	$\max_{k,l} \mathbf{X}_{kl} $	1	$\max_{k,l} \mathbf{X}_{kl} $	1
Absmax	$\max_{k,l} \mathbf{X}_{kl} $	$-\frac{\text{FP4 max}}{(Z(\mathbf{X}))^2} (\text{sign}(\mathbf{X}_{i^*j^*}) \cdot \delta_{ii^*} \delta_{jj^*})$	$\max_{k,l} \mathbf{X}_{kl} $	$\text{sign}(\mathbf{X}_{i^*j^*}) \cdot \delta_{ii^*} \delta_{jj^*}$
Softmax	$\frac{1}{\beta} \log \left(\sum_{k,l} e^{\beta \mathbf{X}_{kl} } \right)$	$-\frac{\text{FP4 max}}{(Z(\mathbf{X}))^2} (\text{softmax}(\beta \mathbf{X})_{ij} \cdot \text{sign}(\mathbf{X}_{ij})) \frac{1}{\beta} \log \left(\sum_{k,l} e^{\beta \mathbf{X}_{kl} } \right)$	$\text{softmax}(\beta \mathbf{X})_{ij} \cdot \text{sign}(\mathbf{X}_{ij})$	
Hybrid	$\max_{k,l} \mathbf{X}_{kl} $	$-\frac{\text{FP4 max}}{(Z(\mathbf{X}))^2} (\text{softmax}(\beta \mathbf{X})_{ij} \cdot \text{sign}(\mathbf{X}_{ij})) \max_{k,l} \mathbf{X}_{kl} $	$\text{softmax}(\beta \mathbf{X})_{ij} \cdot \text{sign}(\mathbf{X}_{ij})$	

For any softmax-based configuration, we must either compute or save the softmax for the backwards pass, incurring additional time and memory complexity. For *Absmax*, it suffices to save the index of the maximum value. For the STE case of $\frac{\partial s}{\partial \mathbf{X}_{ij}}$, we are effectively setting the entire second term from Equation (1), $\left[\frac{q'(s)}{s_q} \left(\mathbf{X}_{ij} Q'(s_q \mathbf{X}_{ij}) - \frac{1}{s_q} Q(s_q \mathbf{X}_{ij}) \right) \right]$, to be equal to 1. This provides a simple alternative to completely omit the $\mathcal{O}(3mn)$ extra computation of this extra gradient term, treating the complex scaling derivative as a direct pass-through. We have an `ignore` option for the $\frac{\partial g}{\partial \mathbf{X}_{ij}}$ term, which means setting the corresponding update term from Corollary 1 to zero: $\frac{\partial g}{\partial \mathbf{X}_{ij}} \left(f_{ij}(\mathbf{U}_p) - \mathbf{U}_{p,ij} \frac{\partial f_{ij}}{\partial \mathbf{U}_{p,ij}} \right) = 0$, skipping the extra $\mathcal{O}(4mn)$ work and saving memory.

6 OTHER TECHNIQUES

Optimizer centric Recently, Huang et al. (2025) proposed StableSPAM, which modifies the Adam optimiser by bounding the momentum term with a moving average statistic. This is motivated by the

observation that in low precision, the gradient norms tend to explode during training, meaning more careful normalisation of the momentum norm and bounding of large values is needed to stabilise training. While their optimiser is primarily tailored around LLMs, we explore the impact of combining StableSPAM with existing rounding and gradient adjustment based techniques for general purpose ML workloads.

Loss scaling We consider loss scaling as a technique to propagate signal when the range of the precision is very limited following Micikevicius et al. (2018). We implement the automated loss scaling technique, which adjusts the loss scaling scale dynamically during training.

Outlier concentration During quantisation, outliers in high-precision may induce quantisation error as they impact the scaling during quantisation. Recent work by Tseng et al. (2024; 2025) proposes applying $Q(\mathbf{HSX}_p)$ to concentrate outliers towards the median of the data. Here \mathbf{HS} is the random Hadamard transform applied to each block \mathbf{X}_p of size l elements, inducing a $\mathcal{O}(\frac{mn}{l}l \cdot \log(l))$ compute overhead. It should be noted that this operation is fusible, and can be done on-the-fly with warp shuffle operations. We consider applying Hadamard transformation in both the forward and backward pass and only the backward pass, akin to Tseng et al. (2024; 2025); Castro et al. (2025).

Spectral decomposition In Li et al. (2025); Cao et al. (2025), they propose to use spectral decomposition techniques to alleviate the difficulty of quantising outliers in low-precision. This is done by decomposing the tensor into a low-rank representation using *singular value decomposition* (SVD), where the low-rank components are then quantised instead. As this is non-fusible, and has prohibitive time complexity overhead $\mathcal{O}(mnk)$ (with k referring to a chosen lower rank), we do not consider it for our simulations as the Hadamard transformation offers a more seamless alternative in the pre-training setting.

Table 2: Summary of FP4 Training Techniques and Overheads. Here we assume each operation is applied to a tensor with n elements, which can be partitioned to $n//l$ blocks with block size l .

Technique	Compute Overhead	Additional Memory	Fuseability	Comment
Straight-Through Estimator (STE)	$\mathcal{O}(1)$	None	Yes	
Baseline $Q'(\mathbf{X})$ Wang et al. (2025)	$\mathcal{O}(n \cdot w \log k)$	$\mathcal{O}(n)$	No	$w = 5$
Spline $Q'(\mathbf{X})$	$\mathcal{O}(n \log k)$	$\mathcal{O}(n)$	No	
Stochastic Rounding Fitzgibbon & Felix (2025)	$\mathcal{O}(n)$	None	Yes	
Stochastic Rounding Scale	$\mathcal{O}(n//l)$	None	Yes	
Global Tensor Scaling Blake et al. (2023)	$\mathcal{O}(n)$	$\mathcal{O}(1)$	Yes	Rescale in full prec.
Global Scaling Gradient (Corollary 1)	$\mathcal{O}(3n)$	$\mathcal{O}(3n)$	No	Save ex. tensor
Differentiable Scale (Absmax)	$\mathcal{O}(4n)$	$\mathcal{O}(3n)$	No	
Differentiable Scale (Softmax)	$\mathcal{O}(4n)$	$\mathcal{O}(4n)$	No	Softmax backw.
Scale Gradient Adjustment	$\mathcal{O}(n)$	$\mathcal{O}(n//l)$	No	Only for Diff. Scale
Outlier concentration (Hadamard) Tseng et al. (2025)	$\mathcal{O}(n \cdot \log l)$	None	Yes	On-the-fly possible
StableSPAM Optimizer Huang et al. (2025)	$\mathcal{O}(n)$	$\mathcal{O}(1)$	No	
Dynamic Loss Scaling Micikevicius et al. (2018)	$\mathcal{O}(n)$	$\mathcal{O}(1)$	No	Mult. each tensor
SVD techniques Li et al. (2025); Cao et al. (2025)	$\mathcal{O}(nk)$	$\mathcal{O}(k^2)$	No	

7 EXPERIMENTS

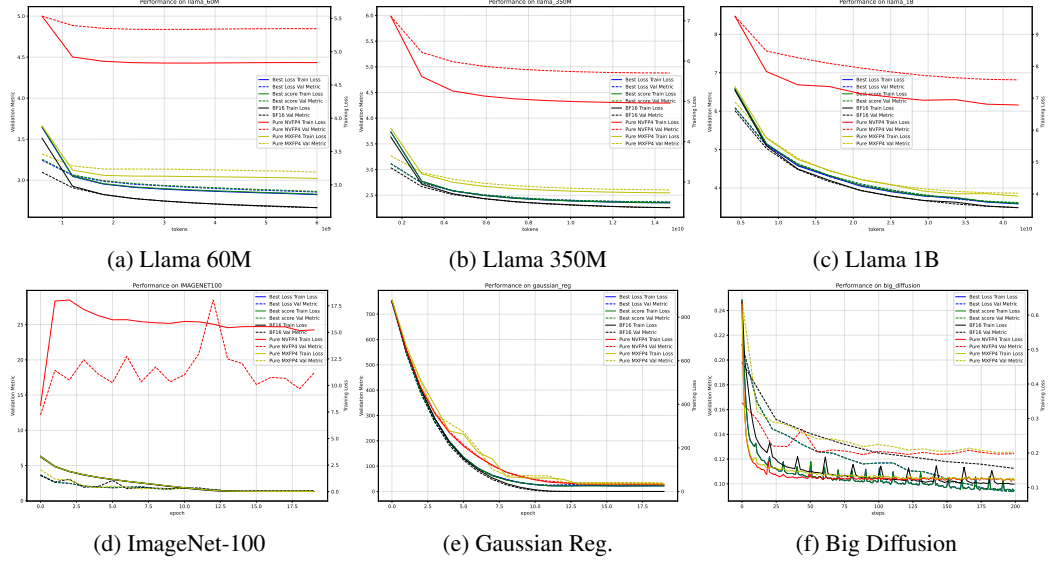
Experimental design and selection strategy We consider the search space in Appendix Table 10, which totals to over 20,000 different parameter combinations, an infeasible search space for larger models. Consequently, our strategy is to do larger sweeps for smaller models that are faster to train and using the results to derive insights and prune the search space for larger models. We run the experiments in the order described in Appendix Table 11.

Performance–efficiency score We define an efficiency score $S(c) = \frac{G(c)}{1+\Omega(c)}$, for a configuration c , that balances relative performance gain $G(c) = (M_{\text{ref}} - M_c)/M_{\text{ref}}$ against a complexity penalty $\Omega(c) = \sum_{t \in \mathcal{T}_c} w_t$. Here, \mathcal{T}_c is the set of non-standard techniques used, w_t their overhead points, and the $+1$ ensures a well-defined score for baseline configurations. Scores are split by positive/negative gain per format, guiding pruning toward configurations that maximize performance with minimal added complexity (see Section .6 for more details). We consider validation loss for M when we calculate the score.

7.1 RESULTS

We loss curves of ImageNet-100, Gaussian regression, U-net large (big_diffusion) and Llama 60M, 350M and 1B in Figure 3. For detailed results of each dataset we refer to Sections .2 and .5. Based on our learnings from experiments, we present three guiding principles when training in FP4.

Figure 3: Training and validation performance curves for selected models and datasets.



Principle 1: Gradient Stability Outweighs Unbiasedness Across all our experiments (Section .2) we found that none of the proposed gradient adjustment had any significant positive effect on training stability compared to STE and consequently we were unable to match the findings in Wang et al. (2025). As a possible explanation for this, consider the `absmax` gradient (Corollary 2), which is a single non-zero entry per block. This mathematically enforces a sparse, high-variance update signal that may introduce high-variance, impacting momentum based optimisers such as Adam or StableSPAM. We also observed this when experimenting with $Q'(\mathbf{X})$, that adding this gradient without lower and upper bound clipping of the relaxation (see Figure 1c) ended up masking out the downstream signal. Consequently using STE, which offers a dense and stable update and led to more stable training in the low-precision context.

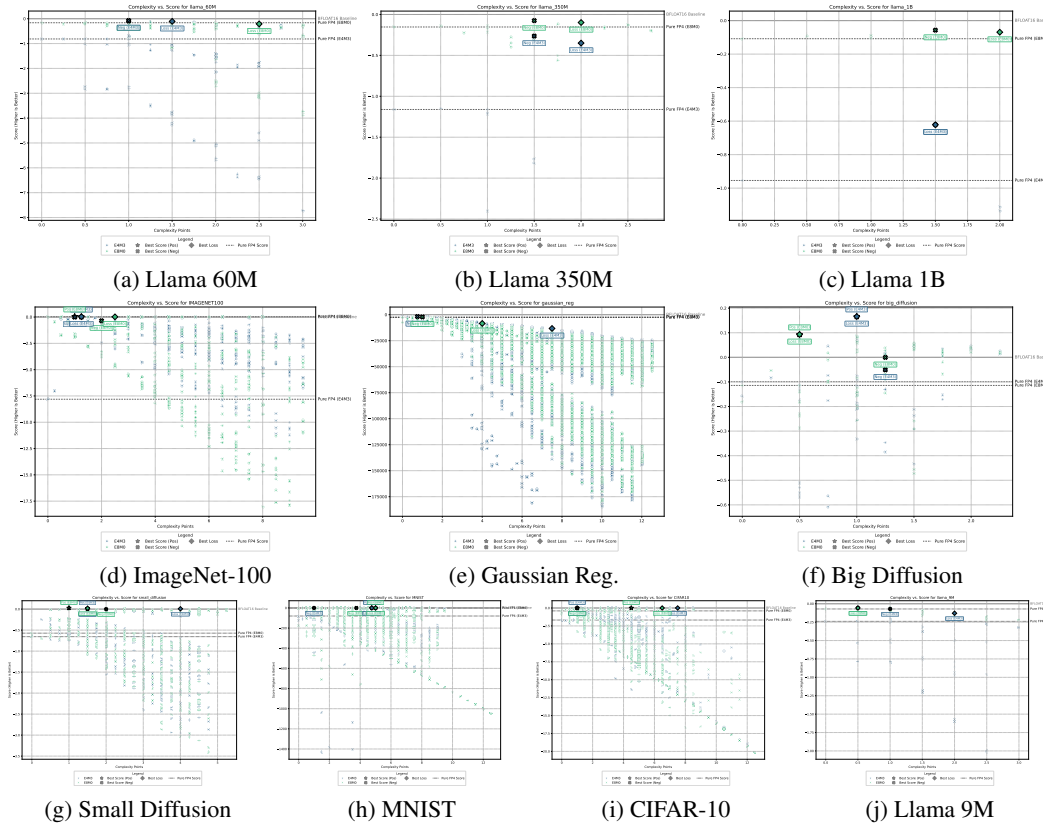
Principle 2: Scale Representation is the Primary Bottleneck We find throughout our experiments and ablations studies that the range of the scaling factor has a profound effect on training stability, especially demonstrated in larger language models and the ImageNet-100 runs in Appendix Tables 3 and 4. As many of our results contradicted findings in Chmiel et al. (2025), we ran ablation studies in Section .3 investigating the additional impact of `SmoothSwiGLU`¹ (Fishman et al., 2025) on language models and ablating the range of E4M3 scaling, by replacing it with E8M3 in Section .4. Our findings suggest that E4M3, despite applying tensor scaling, did not converge due to its range limitation. We speculate that a potential sweet spot exists between E8M0 and E4M3. We then experiment with UE5M3 in Section .5, a format that has increased range and additional precision and find that it indeed consistently outperforms E8M0 on language modelling. The caveat however is that it requires tensor scaling and SR in the backwards pass to achieve this performance. We further find throughout our experiments that nan-handling, also depends on scale format and that it although doesn't have a big impact, it matters.

Principle 3: The Performance-Overhead Frontier is Sparse From our sweeps over thousands of configurations, we find that only a handful of techniques such as Hadamard transforms, tensor scaling, stochastic rounding and optimiser choice provide a consistent, positive return on their

¹This operation adds an approximate $\sim \mathcal{O}(n)$ non-fusable overhead due to additional `absmax` normalisation.

computational overhead. We illustrate this in Pareto-frontier plots in Figure 4 for each dataset and Appendix Figure 10 for the UE5M3 experiments. We overall observe that less complex configurations achieve better scores, and adding complexity yields diminishing returns. One can achieve lower loss, but often at a steep cost with respect to increased overhead, as observed in classification tasks.

Figure 4: Pareto-frontier plots for each dataset, $\Omega(c)$ on the x-axis and $S(c)$ on the y-axis. $S(c) = 0$ implies the configuration c matches BFLOAT16 performance.



Conclusion and further work We've proposed a novel framework for deriving the exact gradient updates for a linear layer under micro-scaling quantisation. While differentiable `absmax` gradients and quantisation gradients provided a benefit on smaller classification tasks, we found they offered no improvement or were detrimental for larger diffusion and language models, suggesting they can often be omitted to reduce overhead without sacrificing performance in these domains. Stochastic rounding of the scale showed little success beyond small models. We further find that the range of NVFP4 hampers its performance on language models, and that the format might require additional overhead inducing adjustments beyond what is presented in Chmiel et al. (2025) for language models up to 1B. We find that UE5M3 scale yields better results than MXFP4, offering a compromise between range and precision, however requiring tensor scaling and SR to work for LLM training, introducing, albeit manageable, overhead. For further research on hardware supporting FP4 training, we'd recommend starting out with MXFP4 and implementing fusible operations such as Hadamard transformation, SR, Tensor scaling, being mindful of nan-handling, carefully selecting the optimiser and finally exploring different scaling formats such as UE5M3. Finally, our work highlights that FP4 training dynamics may not be consistent across model scales, and leave this critical direction to further research.

REFERENCES

Charlie Blake, Douglas Orr, and Carlo Luschi. Unit scaling: Out-of-the-box low-precision training, 2023. URL <https://arxiv.org/abs/2303.11257>.

Rishi Bommasani et al. On the opportunities and risks of foundation models, 2021. URL <https://arxiv.org/abs/2108.07258>.

Hengjie Cao, Mengyi Chen, Yifeng Yang, Ruijun Huang, Fang Dong, Jixian Zhou, Anrui Chen, Mingzhi Dong, Yujiang Wang, Jinlong Hou, Yuan Cheng, Fan Wu, Fan Yang, Tun Lu, Ning Gu, and Li Shang. Metis: Training large language models with advanced low-bit quantization, 2025. URL <https://arxiv.org/abs/2509.00404>.

Roberto L. Castro, Andrei Panferov, Soroush Tabesh, Oliver Sieberling, Jiale Chen, Mahdi Nikdan, Saleh Ashkboos, and Dan Alistarh. Quartet: Native fp4 training can be optimal for large language models, 2025. URL <https://arxiv.org/abs/2505.14669>.

Yuxiang Chen, Haocheng Xi, Jun Zhu, and Jianfei Chen. Oscillation-reduced mxfp4 training for vision transformers, 2025. URL <https://arxiv.org/abs/2502.20853>.

Brian Chmiel, Maxim Fishman, Ron Banner, and Daniel Soudry. Fp4 all the way: Fully quantized training of llms, 2025. URL <https://arxiv.org/abs/2505.19115>.

Eleks Corp. How llms think: Understanding the power of attention mechanisms, 2025. URL <https://eleks.com/blog/how-llms-think/>.

Rares Dolga et al. Latte: Latent attention for linear time transformers, 2024. URL <https://arxiv.org/abs/2402.17512>.

Furkan Duman-Keles et al. On the computational complexity of self-attention. 2023. arXiv preprint arXiv:2301.xxxxx.

Maxim Fishman, Brian Chmiel, Ron Banner, and Daniel Soudry. Scaling fp8 training to trillion-token llms, 2025. URL <https://arxiv.org/abs/2409.12517>.

Andrew Fitzgibbon and Stephen Felix. On stochastic rounding with few random bits, 2025. URL <https://arxiv.org/abs/2504.20634>.

Zhiwei Hao, Jianyuan Guo, Li Shen, Yong Luo, Han Hu, Guoxia Wang, Dianhai Yu, Yonggang Wen, and Dacheng Tao. Low-precision training of large language models: Methods, challenges, and opportunities, 2025. URL <https://arxiv.org/abs/2505.01043>.

Tianjin Huang, Haotian Hu, Zhenyu Zhang, Gaojie Jin, Xiang Li, Li Shen, Tianlong Chen, Lu Liu, Qingsong Wen, Zhangyang Wang, and Shiwei Liu. Stable-spam: How to train in 4-bit more stably than 16-bit adam, 2025. URL <https://arxiv.org/abs/2502.17055>.

Salman Khan, Muzammal Naseer, Munawar Hayat, Syed Waqas Zamir, Fahad Shahbaz Khan, and Mubarak Shah. Transformers in vision: A survey. *ACM Computing Surveys*, 54(10s):1–41, January 2022. ISSN 1557-7341. doi: 10.1145/3505244. URL <http://dx.doi.org/10.1145/3505244>.

Muyang Li, Yujun Lin, Zhekai Zhang, Tianle Cai, Xiuyu Li, Junxian Guo, Enze Xie, Chenlin Meng, Jun-Yan Zhu, and Song Han. Svdquant: Absorbing outliers by low-rank components for 4-bit diffusion models, 2025. URL <https://arxiv.org/abs/2411.05007>.

Paulius Micikevicius, Sharan Narang, Jonah Alben, Gregory Diamos, Erich Elsen, David Garcia, Boris Ginsburg, Michael Houston, Oleksii Kuchaiev, Ganesh Venkatesh, and Hao Wu. Mixed precision training, 2018. URL <https://arxiv.org/abs/1710.03740>.

Paulius Micikevicius, Dusan Stosic, Neil Burgess, Marius Cornea, Pradeep Dubey, Richard Grisenthwaite, Sangwon Ha, Alexander Heinecke, Patrick Judd, John Kamalu, Naveen Mellemudi, Stuart Oberman, Mohammad Shoeybi, Michael Siu, and Hao Wu. Fp8 formats for deep learning, 2022. URL <https://arxiv.org/abs/2209.05433>.

Asit Mishra, Dusan Stosic, and Simon Layton. Recipes for pre-training llms with mxfp8, 2025. URL <https://arxiv.org/abs/2506.08027>.

Badreddine Nouné, Philip Jones, Daniel Justus, Dominic Masters, and Carlo Luschi. 8-bit numerical formats for deep neural networks, 2022. URL <https://arxiv.org/abs/2206.02915>.

Houwen Peng, Kan Wu, Yixuan Wei, Guoshuai Zhao, Yuxiang Yang, Ze Liu, Yifan Xiong, Ziyue Yang, Bolin Ni, Jingcheng Hu, Ruihang Li, Miaosen Zhang, Chen Li, Jia Ning, Ruizhe Wang, Zheng Zhang, Shuguang Liu, Joe Chau, Han Hu, and Peng Cheng. Fp8-lm: Training fp8 large language models, 2023. URL <https://arxiv.org/abs/2310.18313>.

Bita Darvish Rouhani, Ritchie Zhao, Ankit More, Mathew Hall, Alireza Khodamoradi, Summer Deng, Dhruv Choudhary, Marius Cornea, Eric Dellinger, Kristof Denolf, Stosic Dusan, Venmugil Elango, Maximilian Golub, Alexander Heinecke, Phil James-Roxby, Dharmesh Jani, Gaurav Kolhe, Martin Langhammer, Ada Li, Levi Melnick, Maral Mesmakhosroshahi, Andres Rodriguez, Michael Schulte, Rasoul Shafipour, Lei Shao, Michael Siu, Pradeep Dubey, Paulius Mičikevičius, Maxim Naumov, Colin Verrilli, Ralph Wittig, Doug Burger, and Eric Chung. Microscaling data formats for deep learning, 2023. URL <https://arxiv.org/abs/2310.10537>.

Huangyuan Su, Mujin Kwun, Stephanie Gil, Sham Kakade, and Nikhil Anand. Characterization and mitigation of training instabilities in microscaling formats, 2025. URL <https://arxiv.org/abs/2506.20752>.

Xiao Sun, Jungwook Choi, Chia-Yu Chen, Naigang Wang, Swagath Venkataramani, Vijayalakshmi (Viji) Srinivasan, Xiaodong Cui, Wei Zhang, and Kailash Gopalakrishnan. Hybrid 8-bit floating point (hfp8) training and inference for deep neural networks. In H. Wallach, H. Larochelle, A. Beygelzimer, F. d'Alché-Buc, E. Fox, and R. Garnett (eds.), *Advances in Neural Information Processing Systems*, volume 32. Curran Associates, Inc., 2019. URL https://proceedings.neurips.cc/paper_files/paper/2019/file/65fc9fb4897a89789352e211ca2d398f-Paper.pdf.

Albert Tseng, Jerry Chee, Qingyao Sun, Volodymyr Kuleshov, and Christopher De Sa. Quip#: Even better llm quantization with hadamard incoherence and lattice codebooks, 2024. URL <https://arxiv.org/abs/2402.04396>.

Albert Tseng, Tao Yu, and Youngsuk Park. Training llms with mxfp4, 2025. URL <https://arxiv.org/abs/2502.20586>.

Ashish Vaswani et al. Attention is all you need. In *Advances in Neural Information Processing Systems*, 2017.

Ruizhe Wang, Yeyun Gong, Xiao Liu, Guoshuai Zhao, Ziyue Yang, Baining Guo, Zhengjun Zha, and Peng Cheng. Optimizing large language model training using fp4 quantization, 2025. URL <https://arxiv.org/abs/2501.17116>.

Hanmei Yang, Summer Deng, Amit Nagpal, Maxim Naumov, Mohammad Janani, Tongping Liu, and Hui Guan. An Empirical Study of Microscaling Formats for Low-Precision LLM Training . In *2025 IEEE 32nd Symposium on Computer Arithmetic (ARITH)*, pp. 1–8, Los Alamitos, CA, USA, May 2025. IEEE Computer Society. doi: 10.1109/ARITH64983.2025.00011. URL <https://doi.ieee.org/10.1109/ARITH64983.2025.00011>.

Jiecheng Zhou, Ding Tang, Rong Fu, Boni Hu, Haoran Xu, Yi Wang, Zhilin Pei, Zhongling Su, Liang Liu, Xingcheng Zhang, and Weiming Zhang. Towards efficient pre-training: Exploring fp4 precision in large language models, 2025. URL <https://arxiv.org/abs/2502.11458>.

1 LLM USE DISCLOSURE

LLMs were used in writing this paper. LLMs were used to:

1. Polish the writing, wording and condensing text
2. Parse tedious mathematical derivations into latex
3. Parse tedious figures and tables into latex
4. Helping write some of the code

2 EXPERIMENTAL RESULTS

We provide detailed experimental results in this section.

Linear regression We first consider a linear regression task with synthetically generated data $y = X \cdot w_{\text{true}}$ for $X \in \mathbb{R}^{100000 \times 1024}$, $w_{\text{true}} \in \mathbb{R}^{1024 \times 1}$ with $X_{ij}, (w_{\text{true}})_i \stackrel{\text{iid}}{\sim} \mathcal{N}(0, 1)$. We present our results in Table 3. We find that the StableSPAM optimiser finds a perfect solution. We find that stochastic rounding applied to an E4M3 scale yielded the best trade-off in results. Additional gradients resulting from the `absmax` normalisation were not found to be helpful. Overall the StableSPAM optimiser remains the superior choice for regression.

Table 3: Experimental results

Dataset	Source	Val loss	Train loss	Scale	Block size	Max. grad.	Quant. grad	Hadamard	Scale grad	SR	Optimiser	Loss scaling	Round mode	Tensor scaling	Tensor grad	Complexity	Score	NaN mode	
IMAGENET100	Baseline	1.383	0.04	N/A	N/A	N/A	N/A	N/A	N/A	None	Adam	False	N/A	N/A	N/A	N/A	N/A	N/A	
IMAGENET100	Baseline	1.360	0.078	N/A	N/A	N/A	N/A	N/A	N/A	None,exact	StableSPAM	False	N/A	N/A	N/A	N/A	N/A	N/A	
IMAGENET100	Best Score (Neg)	1.391	0.018	E4M3	16	STE	STE	N/A	N/A	None,exact	Adam	True	TiesToPositive	True	ignore	1.000	-0.006	nearest_subnormal	
IMAGENET100	Best Score (Neg)	1.625	0.087	E8M0	32	STE	STE	N/A	N/A	all_activation,exact	StableSPAM	True	TiesToEven	True	ignore	2.000	-0.530	nearest_subnormal	
IMAGENET100	Best Score (Pos)	1.320	0.015	E4M3	16	STE	STE	N/A	N/A	STE	IntelFP4,exact	Adam	True	Stochastic	False	N/A	1.250	0.036	nearest_subnormal
IMAGENET100	Best Score (Pos)	1.317	0.017	E4M3	32	STE	STE	N/A	N/A	STE	None,exact	Adam	True	TiesToPositive	True	ignore	1.000	0.028	nearest_subnormal
IMAGENET100	Best loss MXFP4	1.312	0.014	E8M0	32	STE	STE	N/A	N/A	STE	None,exact	Adam	True	TiesToPositive	True	ignore	2.000	0.020	nearest_subnormal
IMAGENET100	Best loss NVFP4	1.320	0.009	E4M3	16	STE	STE	N/A	N/A	STE	IntelFP4,exact	Adam	True	Stochastic	False	N/A	1.250	0.036	to_0
IMAGENET100	Pure FP4	12.188	8.115	E4M3	16	STE	STE	N/A	N/A	STE	None,exact	Adam	False	TiesToEven	False	N/A	0.000	-7.814	nearest_subnormal
IMAGENET100	Pure FP4	1.344	0.04	E8M0	32	STE	STE	N/A	N/A	STE	None,exact	Adam	False	TiesToEven	False	N/A	0.000	0.028	nearest_subnormal
big_diffusion	Baseline	0.110	0.128	N/A	N/A	N/A	N/A	N/A	N/A	None	Adam	False	N/A	N/A	N/A	N/A	N/A	N/A	
big_diffusion	Baseline	0.113	0.110	N/A	N/A	N/A	N/A	N/A	N/A	None	StableSPAM	False	N/A	N/A	N/A	N/A	N/A	N/A	
big_diffusion	Best Score (Neg)	0.117	0.110	E4M3	16	STE	STE	N/A	N/A	STE	IntelFP4,exact	Adam	True	Stochastic	False	N/A	1.250	-0.051	nearest_subnormal
big_diffusion	Best Score (Neg)	0.113	0.108	E8M0	32	STE	STE	N/A	N/A	STE	all_activation,exact	StableSPAM	False	Stochastic	False	N/A	1.250	-0.000	nearest_subnormal
big_diffusion	Best Score (Pos)	0.094	0.088	E4M3	16	STE	STE	N/A	N/A	STE	None,exact	StableSPAM	False	TiesToEven	True	ignore	1.000	0.160	nearest_subnormal
big_diffusion	Best Score (Pos)	0.092	0.085	E8M0	32	STE	STE	N/A	N/A	STE	None,exact	StableSPAM	False	TiesToEven	True	ignore	0.500	0.093	nearest_subnormal
big_diffusion	Best loss MXFP4	0.102	0.095	E8M0	32	STE	STE	N/A	N/A	STE	None,exact	StableSPAM	False	TiesToEven	False	ignore	0.500	0.093	nearest_subnormal
big_diffusion	Best loss NVFP4	0.094	0.088	E4M3	16	STE	STE	N/A	N/A	STE	None,exact	StableSPAM	False	TiesToEven	True	ignore	1.000	0.166	nearest_subnormal
big_diffusion	Pure FP4	0.124	0.117	E4M3	16	STE	STE	N/A	N/A	STE	None,exact	Adam	False	TowardPositive	False	N/A	0.000	-0.099	nearest_subnormal
big_diffusion	Pure FP4	0.124	0.117	E4M3	32	STE	STE	N/A	N/A	STE	None,exact	Adam	False	TowardPositive	False	N/A	0.000	-0.100	nearest_subnormal
gaussian_rg	Baseline	25.250	25.224	N/A	N/A	N/A	N/A	N/A	N/A	None	Adam	False	N/A	N/A	N/A	N/A	N/A	N/A	
gaussian_rg	Baseline	0.013	0.013	N/A	N/A	N/A	N/A	N/A	N/A	None	StableSPAM	False	N/A	N/A	N/A	N/A	N/A	N/A	
gaussian_rg	Best Score (Neg)	23.500	24.875	E4M3	16	STE	STE	N/A	N/A	STE	None,exact	StableSPAM	False	Stochastic	False	N/A	0.750	-1815.151	nearest_subnormal
gaussian_rg	Best Score (Neg)	27.875	27.928	E8M0	32	STE	STE	N/A	N/A	STE	None,exact	StableSPAM	False	TowardPositive	True	ignore	1.000	-2153.264	nearest_subnormal
gaussian_rg	Best Score (Pos)	27.875	27.928	E8M0	32	STE	STE	N/A	N/A	STE	None,exact	StableSPAM	False	TowardPositive	True	ignore	0.000	0.000	nearest_subnormal
gaussian_rg	Best loss MXFP4	27.875	27.928	E8M0	32	STE	STE	N/A	N/A	STE	None,exact	StableSPAM	False	TiesToEven	True	ignore	7.500	-13251.368	nearest_subnormal
gaussian_rg	Best loss NVFP4	27.875	27.928	E4M3	16	STE	STE	N/A	N/A	STE	None,exact	StableSPAM	True	TiesToEven	True	ignore	0.000	-2327.151	nearest_subnormal
gaussian_rg	Pure FP4	30.125	30.947	E4M3	16	STE	STE	N/A	N/A	STE	None,exact	Adam	False	TiesToEven	False	N/A	0.000	-2626.623	nearest_subnormal
gaussian_rg	Pure FP4	34.000	34.303	E8M0	32	STE	STE	N/A	N/A	STE	None,exact	Adam	False	TiesToEven	False	N/A	0.000	-2626.623	nearest_subnormal

Image classification We find in Table 3 and Appendix Table 5, that any max relaxation had no effect on performance. Here we find that in some cases using `absmax` in the tensor scaling gradient tends to help. We generally find that stochastic rounding, combined with tensor scaling and loss scaling leads to the most effective improvements. Here Adam seems to work better overall. We observe that NVFP4 does not work out of the box while MXFP4 does.

Diffusion We find in Table 3 and and Appendix Table 5 that any application of `absmax` gradients does not have any positive effect. We find that it suffices to use loss and tensor scaling combined with the StableSPAM optimiser to achieve a good performance.

LLM We present our results in Table 4 and Figure 3. We are unable to reproduce the findings of Chmiel et al. (2025), where we contrastingly find MXFP4 to outperform NVFP4 for LLM training. We note that Fishman et al. (2025) additionally uses `SmoothSwiGLU` Fishman et al. (2025) in their experiments which induces a non-fusable $\mathcal{O}(n)$ overhead as it requires the `absmax` along one dimension of the tensor, which we have omitted in our main experiments. We include this in further experiments in Section .3 and find that it marginally improves performance, but still fails for the 1B model.

In contrast to Tseng et al. (2025); Castro et al. (2025), we did not find that the combination of Hadamard transformation and SR yielded a significantly better result for MXFP4, suggesting that SR can possibly be omitted to reduce overhead. We do not find that the relaxation of quantisation gradients proposed in Zhou et al. (2025) had any impact on stabilizing the training of LLMs.

Exploring UE5M3 scale format We find in ablation studies (see Section .4) for E4M3, that the limiting factor during LLM training (with tensor scaling only) is the range of the exponent. We

Table 4: LLM results

Dataset	Source	Val loss	Train loss	Scale	Block size	Max. grad.	Quant. grad.	Hadamard	Scale grad	SR	Optimiser	Loss scaling	Round mode	Tensor scaling	Tensor grad	Complexity points	Score	NaN mode	
llama,1B	Baseline	3.578	3.692	N/A	N/A	N/A	N/A	N/A	N/A	N/A	Adam	False	N/A	N/A	N/A	N/A	N/A		
llama,1B	Baseline	3.487	3.569	N/A	N/A	N/A	N/A	N/A	N/A	StableSPAM	False	N/A	N/A	N/A	N/A	N/A			
llama,1B	Best Score (Neg)	4.933	4.957	E4M3	16	STE	STE	N/A	STE	None,exact	StableSPAM	True	TiesToEven	True	ignore	1.500	0.632	nearest,subnormal	
llama,1B	Best Score (Neg)	3.620	3.701	ERMO	32	STE	STE	all,exact	STE	None,exact	StableSPAM	False	TiesToEven	False	N/A	1.500	-0.057	nearest,subnormal	
llama,1B	Best loss MXFP4	3.608	3.688	ERMO	32	STE	STE	all,exact	STE	None,exact	StableSPAM	True	TiesToEven	False	N/A	2.000	-0.069	nearest,subnormal	
llama,1B	Best loss NVFP4	4.933	4.957	E4M3	16	STE	STE	N/A	STE	None,exact	StableSPAM	True	TiesToEven	True	ignore	1.500	-0.622	nearest,subnormal	
llama,1B	Pure FP4	6.815	6.789	E4M3	16	STE	STE	N/A	STE	None,exact	Adam	False	TiesToEven	False	N/A	0.000	-0.954	nearest,subnormal	
llama,1B	Pure FP4	3.864	3.932	ERMO	32	STE	STE	N/A	STE	None,exact	Adam	False	TiesToEven	False	N/A	0.000	-0.108	nearest,subnormal	
llama,1B	Pure FP4	2.509	2.373	N/A	N/A	N/A	N/A	N/A	N/A	N/A	N/A	N/A	N/A	N/A	N/A	N/A	N/A		
llama,350M	Baseline	2.558	2.563	N/A	N/A	N/A	N/A	N/A	N/A	N/A	N/A	N/A	N/A	N/A	N/A	N/A	N/A		
llama,350M	Best Score (Neg)	2.655	2.783	E4M3	16	STE	STE	N/A	STE	None,exact	IntelfP4,exact	False	TiesToEven	False	N/A	2.000	-0.098	nearest,subnormal	
llama,350M	Best loss NVFP4	2.371	2.485	ERMO	32	STE	STE	all,exact	STE	None,exact	StableSPAM	False	TiesToEven	True	ignore	1.500	-0.264	nearest,subnormal	
llama,350M	Best loss MXFP4	2.369	2.483	ERMO	32	STE	STE	all,exact	STE	None,exact	StableSPAM	False	TiesToEven	True	ignore	1.500	-0.075	nearest,subnormal	
llama,350M	Pure FP4	2.653	2.781	E4M3	16	STE	STE	N/A	STE	None,exact	IntelfP4,exact	False	TiesToEven	True	ignore	2.000	-0.350	nearest,subnormal	
llama,350M	Pure FP4	2.480	2.774	ERMO	32	STE	STE	N/A	STE	None,exact	Adam	False	TiesToEven	False	N/A	0.000	-0.153	nearest,subnormal	
llama,350M	Pure FP4	2.665	2.557	N/A	N/A	N/A	N/A	N/A	N/A	N/A	N/A	N/A	N/A	N/A	N/A	N/A	N/A		
llama,60M	Baseline	2.983	3.028	N/A	N/A	N/A	N/A	N/A	N/A	N/A	StableSPAM	False	N/A	N/A	N/A	N/A	N/A		
llama,60M	Best Score (Neg)	2.864	2.860	E4M3	16	STE	STE	N/A	STE	None,exact	IntelfP4,exact	Adam	False	TiesToEven	True	ignore	1.000	-0.074	nearest,subnormal
llama,60M	Best Score (Neg)	2.917	2.908	ERMO	32	STE	STE	all,exact	STE	None,exact	Adam	False	TiesToEven	False	N/A	1.000	-0.094	nearest,subnormal	
llama,60M	Best loss NVFP4	2.889	2.880	ERMO	32	STE	STE	all,exact	STE	None,exact	StableSPAM	True	TiesToEven	True	ignore	2.500	-0.210	to_one	
llama,60M	Best loss NVFP4	2.856	2.852	E4M3	16	STE	STE	N/A	STE	None,exact	IntelfP4,exact	StableSPAM	False	TiesToEven	True	ignore	1.500	-0.107	nearest,subnormal
llama,60M	Pure FP4	4.838	4.829	E4M3	16	STE	STE	N/A	STE	None,exact	Adam	False	TiesToEven	False	N/A	0.000	-0.815	nearest,subnormal	
llama,60M	Pure FP4	3.099	3.096	ERMO	32	STE	STE	N/A	STE	None,exact	Adam	False	TiesToEven	False	N/A	0.000	-0.163	nearest,subnormal	

explore whether an alternative format like UE5M3 can achieve better performance than MXFP 4 in Section 5. Our results suggest that UE5M3 offers a good compromise, with improved performance compared to E8M0 scale on language modelling tasks. A caveat however is that UE5M3 needs tensor scaling and SR in the backwards pass to stabilise, and exhibits instability in its pure form, unlike MXFP 4. There is thus a computational overhead needed for the increased precision. We note that the best nan-handling strategy changes to “to_one”.

Additional dataset results We present the additional results for MNIST, CIFAR10, Llama 9M and Small U-net (CIFAR 10) in Figure 5 and Table 5.

Figure 5: Training and validation performance curves for other datasets.

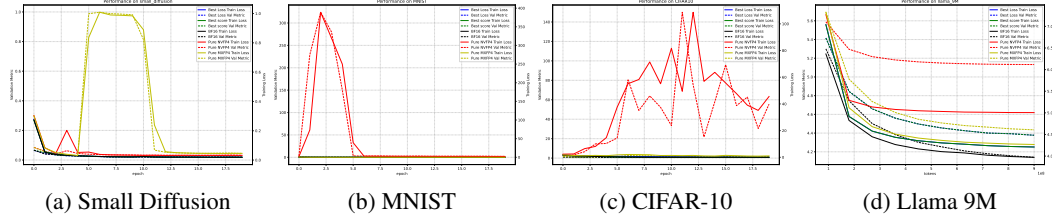


Table 5: Additional experimental results

Dataset	Source	Val loss	Train loss	Scale	Block size	Max. grad.	Quant. grad.	Hadamard	Scale grad	SR	Optimiser	Loss scaling	Round mode	Tensor scaling	Tensor grad	Complexity points	Score	NaN mode	
CIFAR10	Baseline	0.875	0.003	N/A	N/A	N/A	N/A	N/A	N/A	N/A	Adam	False	N/A	N/A	N/A	N/A	N/A		
CIFAR10	Baseline	0.895	0.027	N/A	N/A	N/A	N/A	N/A	N/A	StableSPAM	False	N/A	N/A	N/A	N/A	N/A			
CIFAR10	Best Score (Neg)	0.860	0.003	E4M3	16	STE	STE	N/A	STE	None,exact	Adam	False	TiesToEven	True	ignore	1.000	-0.099	nearest,subnormal	
CIFAR10	Best Score (Neg)	0.883	0.003	ERMO	32	STE	STE	N/A	STE	None,exact	IntelfP4,exact	Adam	True	TiesToEven	False	N/A	1.000	-0.099	nearest,subnormal
CIFAR10	Best Score (Pos)	0.867	0.003	E4M3	16	STE	STE	N/A	STE	all,activation,exact	Adam	True	TiesToEven	False	N/A	1.000	0.009	nearest,subnormal	
CIFAR10	Best Score (Pos)	0.855	0.040	ERMO	32	STE	STE	N/A	STE	all,activation,exact	Adam	True	TiesToEven	True	absmax	4.500	0.005	nearest,subnormal	
CIFAR10	Best loss MXFP4	0.858	0.040	ERMO	32	STE	STE	N/A	STE	all,activation,exact	Adam	True	TiesToEven	True	absmax	6.500	0.003	nearest,subnormal	
CIFAR10	Best loss NVFP4	0.836	0.037	E4M3	16	STE	STE	N/A	STE	None,exact	Adam	True	TowardPositive	True	absmax	7.500	0.003	nearest,subnormal	
CIFAR10	Pure FP4	2.344	2.354	E4M3	16	STE	STE	N/A	STE	None,exact	Adam	False	TowardPositive	False	N/A	0.000	-1.679	nearest,subnormal	
CIFAR10	Pure FP4	0.937	0.007	ERMO	32	STE	STE	N/A	STE	None,exact	Adam	False	TiesToEven	False	N/A	0.000	-0.604	nearest,subnormal	
MNIST	Baseline	0.027	0.016	N/A	N/A	N/A	N/A	N/A	N/A	N/A	Adam	False	N/A	N/A	N/A	N/A	N/A		
MNIST	Baseline	0.028	0.004	N/A	N/A	N/A	N/A	N/A	N/A	StableSPAM	False	N/A	N/A	N/A	N/A	N/A			
MNIST	Best Score (Neg)	0.027	0.008	E4M3	16	STE	STE	N/A	STE	None,exact	StableSPAM	True	TowardPositive	False	N/A	1.000	-0.005	nearest,subnormal	
MNIST	Best Score (Neg)	0.027	0.007	ERMO	32	STE	STE	N/A	STE	None,exact	StableSPAM	True	TowardPositive	True	ignore	3.750	-0.051	nearest,subnormal	
MNIST	Best Score (Pos)	0.010	0.006	E4M3	16	STE	STE	N/A	STE	None,exact	StableSPAM	True	TowardPositive	True	absmax	4.750	0.003	nearest,subnormal	
MNIST	Best Score (Pos)	0.021	0.006	ERMO	32	STE	STE	N/A	STE	None,exact	IntelfP4,exact	StableSPAM	True	TiesToEven	True	absmax	5.000	0.043	nearest,subnormal
MNIST	Best loss MXFP4	0.021	0.006	E4M3	16	STE	STE	N/A	STE	None,exact	IntelfP4,exact	StableSPAM	True	TiesToEven	True	absmax	5.000	0.043	nearest,subnormal
MNIST	Best loss NVFP4	0.021	0.009	E4M3	16	STE	STE	N/A	STE	None,exact	StableSPAM	True	TowardPositive	True	absmax	4.750	0.050	to_one	
MNIST	Pure FP4	2.188	2.258	E4M3	16	STE	STE	N/A	STE	None,exact	Adam	False	TiesToEven	False	N/A	0.000	-0.808	nearest,subnormal	
MNIST	Pure FP4	0.030	0.003	ERMO	32	STE	STE	N/A	STE	None,exact	Adam	False	TiesToEven	False	N/A	0.000	-0.738	nearest,subnormal	
llama,9M	Baseline	1.183	4.013	N/A	N/A	N/A	N/A	N/A	N/A	N/A	Adam	False	N/A	N/A	N/A	N/A	N/A		
llama,9M	Baseline	4.141	3.972	N/A	N/A	N/A	N/A	N/A	N/A	StableSPAM	False	N/A	N/A	N/A	N/A	N/A			
llama,9M	Best Score (Neg)	4.433	4.271	E4M3	16	STE	STE	N/A	STE	None,exact	IntelfP4,exact	Adam	False	TiesToEven	True	ignore	1.000	-0.071	nearest,subnormal
llama,9M	Best Score (Neg)	4.377	4.210	ERMO	32	STE	STE	N/A	STE	None,exact	StableSPAM	False	TiesToEven	False	N/A	0.500	-0.057	nearest,subnormal	
llama,9M	Best loss MXFP4	4.377	4.210	ERMO	32	STE	STE	N/A	STE	None,exact	StableSPAM	False	TiesToEven	False	N/A	0.500	-0.057	nearest,subnormal	
llama,9M	Best loss NVFP4	4.245	4.245	E4M3	16	STE	STE	N/A	STE	None,exact	IntelfP4,exact	StableSPAM	True	TiesToEven	True	ignore	2.000	-0.29	nearest,subnormal
llama,9M	Pure FP4	5.133	4.268	E4M3	16	STE	STE	N/A	STE	None,exact	Adam	False	TiesToEven	False	N/A	0.000	-0.220	nearest,subnormal	
llama,9M	Pure FP4	4.435	4.268	ERMO	32	STE	STE	N/A	STE	None,exact	Adam	False	TiesToEven	False	N/A	0.000	-0.071	nearest,subnormal	
small,diffusion	Baseline	0.029	0.029	N/A	N/A	N/A	N/A	N/A	N/A	N/A	Adam	False	N/A	N/A	N/A	N/A	N/A		
small,diffusion	Best Score (Neg)	0.019	0.019	N/A	N/A	N/A	N/A	N/A	N/A	StableSPAM	False	N/A	N/A	N/A	N/A	N/A			
small,diffusion	Best Score (Pos)	0.019	0.019	E4M3	16	STE	STE	N/A	STE	None,exact	StableSPAM	False	TiesToEven	True	ignore	2.000	-0.057	nearest,subnormal	
small,diffusion	Best Score (Pos)	0.018	0.019	E4M3	16	STE	STE	N/A	STE	None,exact	IntelfP4,exact	StableSPAM	True	TowardPositive	False	N/A	1.500	0.020	nearest,subnormal
small,diffusion	Best Score (Pos)	0.018	0.019	E4M3	16	STE	STE	N/A	STE	None,exact	StableSPAM	False	TiesToEven	False	N/A	1.000	0.028	nearest,subnormal	
small,diffusion	Best loss MXFP4	0.018	0.019	E4M3	16	STE	STE	N/A	STE	None,exact	IntelfP4,exact	StableSPAM	False	TiesToEven	True	ignore	1.500	0.020	to_one
small,diffusion	Best loss NVFP4	0.018	0.019	E4M3	16	STE	STE	N/A	STE	None,exact	Adam	False	TiesToEven	True	ignore	4.000	0.008	nearest,subnormal	
small,diffusion	Pure FP4	0.031	0.031	E4M3	16	STE	STE	N/A	STE	None,exact	Adam	False	TiesToEven	False	N/A	0.000	-0.656	nearest,subnormal	
small,diffusion	Pure FP4	0.030	0.031	ERMO	32	STE	STE	N/A	STE	None,exact	Adam	False	TiesToEven	False	N/A	0.000	-0.572	nearest,subnormal	

3 TESTING SMOOTH SWIGLU, TENSOR SCALING AND SR

We replicate the results in Chmiel et al. (2025) more exactly by adding the SmoothSwiGLU in Fishman et al. (2025). We could not replicate their indicated results on models up to LLama 1B in Figure 6 and Table 6.

Figure 6: Training and validation performance curves LLama with SSWiGLU. The gap between BFLOAT16 still grows with model size despite tensor scaling and SR.

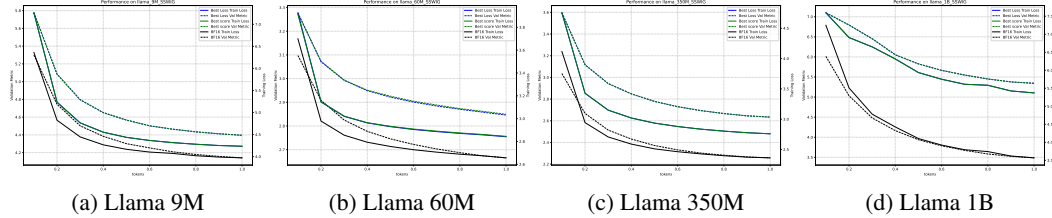


Table 6: SWIG results

Dataset	Source	Val loss	Train loss	Scale	Block size	Max. grad.	Quant. grad.	Hadamard	Scale grad	SR	Optimiser	Loss scaling	Round mode	Tensor scaling	Tensor grad	Complexity points	Score	NaN mode
llama_1B	Baseline	3.578	3.682	N/A	N/A	N/A	N/A	N/A	N/A	Adam	False	N/A	N/A	N/A	N/A	N/A	N/A	N/A
llama_1B	Baseline	3.487	3.569	N/A	N/A	N/A	N/A	N/A	N/A	StableSPAM	False	N/A	N/A	N/A	N/A	N/A	N/A	N/A
llama_1B,SSWIG	Best Score (Neg)	5.343	5.372	E4M3	16	STE	STE	None,exact	STE	None,exact	StableSPAM	False	TiesToEven	True	ignore	1.000	-0.532	to,one
llama_1B,SSWIG	Best loss NVFP4	5.343	5.372	E4M3	16	STE	STE	None,exact	STE	None,exact	StableSPAM	False	TiesToEven	True	ignore	1.000	-0.532	to,one
llama_350M	Baseline	2.269	2.375	N/A	N/A	N/A	N/A	N/A	N/A	Adam	False	N/A	N/A	N/A	N/A	N/A	N/A	N/A
llama_350M	Baseline	2.269	2.375	N/A	N/A	N/A	N/A	N/A	N/A	StableSPAM	False	N/A	N/A	N/A	N/A	N/A	N/A	N/A
llama_350M,SSWIG	Best Score (Neg)	2.634	2.760	E4M3	16	STE	STE	None,exact	STE	None,exact	StableSPAM	False	TiesToEven	True	ignore	1.500	-0.250	to,one
llama_350M,SSWIG	Best loss NVFP4	2.634	2.760	E4M3	16	STE	STE	None,exact	STE	None,exact	StableSPAM	False	TiesToEven	True	ignore	1.500	-0.250	to,one
llama_60M	Baseline	2.665	2.657	N/A	N/A	N/A	N/A	N/A	N/A	Adam	False	N/A	N/A	N/A	N/A	N/A	N/A	N/A
llama_60M	Baseline	2.983	3.028	N/A	N/A	N/A	N/A	N/A	N/A	StableSPAM	False	N/A	N/A	N/A	N/A	N/A	N/A	N/A
llama_409M,SSWIG	Best Score (Neg)	2.849	2.863	E4M3	16	STE	STE	None,exact	STE	None,exact	StableSPAM	False	TiesToEven	True	ignore	1.500	-0.033	nearest,subnormal
llama_409M,SSWIG	Best loss E4M3	2.849	2.863	E4M3	16	STE	STE	None,exact	STE	None,exact	StableSPAM	False	TiesToEven	True	ignore	2.000	-0.130	to,one
llama_9M	Baseline	4.183	4.013	N/A	N/A	N/A	N/A	N/A	N/A	Adam	False	N/A	N/A	N/A	N/A	N/A	N/A	N/A
llama_9M	Baseline	4.141	3.972	N/A	N/A	N/A	N/A	N/A	N/A	StableSPAM	False	N/A	N/A	N/A	N/A	N/A	N/A	N/A
llama_9M,SSWIG	Best Score (Neg)	4.396	4.235	E4M3	16	STE	STE	None,exact	STE	None,exact	StableSPAM	False	TiesToEven	True	ignore	1.500	-0.092	nearest,subnormal
llama_9M,SSWIG	Best loss NVFP4	4.396	4.235	E4M3	16	STE	STE	None,exact	STE	None,exact	StableSPAM	False	TiesToEven	True	ignore	1.500	-0.092	nearest,subnormal

4 CHANGING THE SCALE TO E8M3

During our experiments, we noticed that E4M3 did not match the performance of E8M0, even with tensor scaling. We speculated that the range of E4M3 was the issue and decided to verify this with an ablation study using E8M3 to test this hypothesis. We presents the results in Table 7 and Figure 7.

Table 7: E8M3 ablation results

Dataset	Source	Val loss	Train loss	Scale	Block size	Max. grad.	Quant. grad.	Hadamard	Scale grad	SR	Optimiser	Loss scaling	Round mode	Tensor scaling	Tensor grad	Complexity points	Score	NaN mode	
llama_60M	Baseline	2.665	2.657	N/A	N/A	N/A	N/A	N/A	N/A	Adam	False	N/A	N/A	N/A	N/A	N/A	N/A	N/A	
llama_60M	Baseline	2.983	3.028	N/A	N/A	N/A	N/A	N/A	N/A	StableSPAM	False	N/A	N/A	N/A	N/A	N/A	N/A	N/A	
llama_60M	Best Score (Neg)	2.775	2.773	E8M3	16.000	STE	STE	None,exact	STE	None,exact	IntelFP4,exact	StableSPAM	False	TiesToEven	False	N/A	1.000	-0.041	nearest,subnormal
llama_60M	Best loss E8M3	2.775	2.773	E8M3	16.000	STE	STE	None,exact	STE	None,exact	IntelFP4,exact	StableSPAM	False	TiesToEven	False	N/A	1.000	-0.041	nearest,subnormal
llama_60M	Best loss NVFP4	2.775	2.773	E8M3	16.000	STE	STE	None,exact	STE	None,exact	IntelFP4,exact	StableSPAM	False	TiesToEven	False	N/A	0.000	-0.070	nearest,subnormal
llama_9M	Baseline	4.183	4.013	N/A	N/A	N/A	N/A	N/A	N/A	Adam	False	N/A	N/A	N/A	N/A	N/A	N/A	N/A	
llama_9M	Baseline	4.141	3.972	N/A	N/A	N/A	N/A	N/A	N/A	StableSPAM	False	N/A	N/A	N/A	N/A	N/A	N/A	N/A	
llama_9M	Best Score (Neg)	4.271	4.106	E8M3	16.000	STE	STE	None,exact	STE	None,exact	IntelFP4,exact	StableSPAM	False	TiesToEven	False	N/A	1.000	-0.031	nearest,subnormal
llama_9M	Best loss E8M3	4.271	4.106	E8M3	16.000	STE	STE	None,exact	STE	None,exact	IntelFP4,exact	StableSPAM	False	TiesToEven	False	N/A	1.000	-0.031	nearest,subnormal
llama_9M	Pure FP4	4.320	4.156	E8M3	16.000	STE	STE	None,exact	STE	None,exact	Adam	False	TiesToEven	False	N/A	0.000	-0.043	nearest,subnormal	

Confirming that the limiting factor of E4M3 is the range, we next speculate that an 8-bit numerical scaling format in-between E4M3 and E8M0 might offer a good trade-off between range and precision.

5 UE5M3 RESULTS

We present the UE5M3 experiments in Table 8. We overall find that the UE5M3 outperforms MXFP 4 when tensor scaling is applied. It should be noted that UE5M3 will not work without any adjustments unlike MXFP 4, implying that increased precision often comes with increased overhead. We visualise the training and validation curves in Figure 8 and Figure 9. We further provide the Pareto-frontier plots in Figure 10, we note that generally lower complexity configurations achieve better scores.

Figure 7: Training and validation performance curves for E8M3.

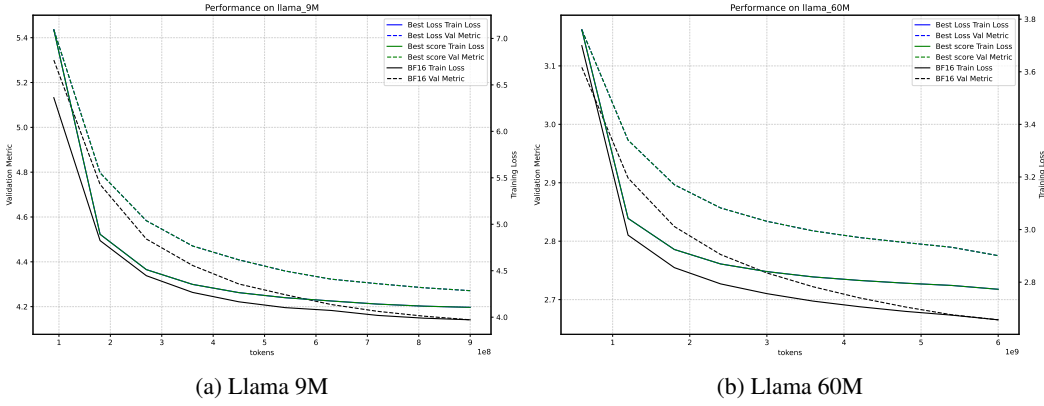


Table 8: UE5M3 results

Dataset	Source	Val loss	Train loss	Scale	Block size	Max. grad.	Quant.	Hadamard	Scale grad	SR	Optimizer	Loss scaling	Round mode	Tensor scaling	Tensor grad	Complexity points	Score	NaN mode
CIFAR10	Baseline	0.25	0.03	N/A	N/A	N/A	N/A	N/A	N/A	Adam	False	N/A	N/A	N/A	N/A	N/A	N/A	N/A
CIFAR10	Baseline	0.895	0.027	N/A	N/A	N/A	N/A	N/A	N/A	StableSPAM	False	N/A	N/A	N/A	N/A	N/A	N/A	N/A
CIFAR10	Best Score (Neg)	0.883	0.003	ESM3	32	STE	STE	None,exact	STE	IntelFP,exact	Adam	True	TiesToEven	False	N/A	1.000	-0.009	nearest_subnormal
CIFAR10	Best Score (Pos)	0.867	0.003	ESM3	32	STE	STE	None,exact	STE	IntelFP,exact	Adam	Fals	TiesToEven	False	N/A	0.500	0.009	nearest_subnormal
CIFAR10	Best loss ESM3	0.867	0.003	ESM3	32	STE	STE	None,exact	STE	IntelFP,exact	Adam	Fals	TiesToEven	False	N/A	0.500	0.009	nearest_subnormal
CIFAR10	Pure FP4	0.875	0.005	ESM2	32	STE	STE	None,exact	STE	None,exact	Adam	Fals	TowardPositive	False	N/A	0.000	0.000	nearest_subnormal
CIFAR10	Pure FP4	0.875	0.005	ESM2	32	STE	STE	None,exact	STE	None,exact	Adam	Fals	TiesToEven	False	N/A	0.000	0.018	nearest_subnormal
IMAGENET100	Baseline	1.383	0.014	N/A	N/A	N/A	N/A	N/A	N/A	Adam	False	N/A	N/A	N/A	N/A	N/A	N/A	N/A
IMAGENET100	Baseline	1.750	0.076	N/A	N/A	N/A	N/A	N/A	N/A	StableSPAM	False	N/A	N/A	N/A	N/A	N/A	N/A	N/A
IMAGENET100	Best Score (Neg)	1.391	0.015	ESM3	32	STE	STE	None,exact	STE	all.activation,exact	Adam	True	TowardPositive	False	N/A	1.000	-0.006	nearest_subnormal
IMAGENET100	Best Score (Pos)	1.346	0.015	ESM3	32	STE	STE	None,exact	STE	IntelFP,exact	Adam	Fals	TiesToEven	False	N/A	0.500	0.028	nearest_subnormal
IMAGENET100	Best loss ESM3	1.344	0.014	ESM3	32	STE	STE	None,exact	STE	IntelFP,exact	Adam	Fals	TiesToEven	False	N/A	0.500	0.028	nearest_subnormal
IMAGENET100	Pure FP4	2.031	1.530	ESM3	32	STE	STE	None,exact	STE	None,exact	Adam	Fals	TowardPositive	False	N/A	0.000	-0.469	nearest_subnormal
MNIST	Baseline	0.027	0.016	N/A	N/A	N/A	N/A	N/A	N/A	Adam	Fals	N/A	N/A	N/A	N/A	N/A	N/A	N/A
MNIST	Best Score (Neg)	0.028	0.004	N/A	N/A	N/A	N/A	N/A	N/A	StableSPAM	False	TiesToEven	True	ignore	1.000	-0.003	nearest_subnormal	
MNIST	Best Score (Pos)	0.025	0.006	ESM3	32	STE	STE	None,exact	STE	IntelFP,exact	StableSPAM	False	TiesToEven	True	ignore	1.250	0.047	nearest_subnormal
MNIST	Best loss ESM3	0.025	0.006	ESM3	32	STE	STE	None,exact	STE	IntelFP,exact	StableSPAM	False	Stochastic	Fals	N/A	1.250	0.047	nearest_subnormal
MNIST	Pure FP4	0.029	0.022	ESM2	16	STE	STE	None,exact	STE	None,exact	Adam	Fals	TowardPositive	False	N/A	0.000	-0.059	nearest_subnormal
MNIST	Pure FP4	0.029	0.022	ESM2	16	STE	STE	None,exact	STE	None,exact	Adam	Fals	TiesToEven	False	N/A	0.000	-0.072	nearest_subnormal
big_diffusion	Baseline	0.3	0.08	N/A	N/A	N/A	N/A	N/A	N/A	StableSPAM	False	N/A	N/A	N/A	N/A	N/A	N/A	N/A
big_diffusion	Baseline	0.313	0.110	N/A	N/A	N/A	N/A	N/A	N/A	StableSPAM	False	N/A	N/A	N/A	N/A	N/A	N/A	N/A
big_diffusion	Best Score (Neg)	0.113	0.109	ESM3	32	STE	STE	None,exact	STE	None,exact	Adam	True	Stochastic	Fals	N/A	0.750	-0.006	nearest_subnormal
big_diffusion	Best Score (Pos)	0.101	0.106	ESM3	32	STE	STE	None,exact	STE	all.activation,exact	StableSPAM	False	TowardPositive	False	N/A	1.000	0.074	to_one
big_diffusion	Best loss ESM3	0.102	0.097	ESM3	32	STE	STE	None,exact	STE	all.activation,exact	StableSPAM	True	TiesToEven	False	N/A	1.500	0.062	to_one
big_diffusion	Pure FP4	0.250	0.253	ESM3	32	STE	STE	None,exact	STE	None,exact	Adam	Fals	TiesToEven	False	N/A	0.000	0.104	nearest_subnormal
gaussian_nz	Baseline	0.250	0.224	N/A	N/A	N/A	N/A	N/A	N/A	Adam	False	N/A	N/A	N/A	N/A	N/A	N/A	N/A
gaussian_nz	Baseline	0.013	0.013	N/A	N/A	N/A	N/A	N/A	N/A	StableSPAM	False	N/A	N/A	N/A	N/A	N/A	N/A	N/A
gaussian_nz	Best Score (Neg)	0.285	0.023	ESM3	32	STE	STE	None,exact	STE	IntelFP,exact	StableSPAM	False	TiesToEven	True	ignore	1.000	-1998.698	nearest_subnormal
gaussian_nz	Best Score (Pos)	0.250	0.023	ESM3	32	STE	STE	backward,exact	STE	IntelFP,exact	StableSPAM	True	Stochastic	True	ignore	3.250	-6338.788	nearest_subnormal
gaussian_nz	Best loss ESM3	0.250	0.024	ESM3	32	STE	STE	None,exact	STE	IntelFP,exact	StableSPAM	False	Fals	N/A	0.000	0.000	0.000	nearest_subnormal
gaussian_nz	Pure FP4	0.375	0.383	ESM3	32	STE	STE	None,exact	STE	None,exact	Adam	Fals	TiesToEven	False	N/A	0.000	-2423.785	nearest_subnormal
llama_1B	Baseline	3.578	3.682	N/A	N/A	N/A	N/A	N/A	N/A	Adam	Fals	N/A	N/A	N/A	N/A	N/A	N/A	N/A
llama_1B	Baseline	3.487	3.569	N/A	N/A	N/A	N/A	N/A	N/A	StableSPAM	False	N/A	N/A	N/A	N/A	N/A	N/A	N/A
llama_1B	Best Score (Neg)	3.586	3.497	ESM3	32	STE	STE	None,exact	STE	IntelFP,exact	StableSPAM	False	TiesToEven	True	ignore	1.500	-0.043	to_one
llama_1B	Best Score (Pos)	3.566	3.497	ESM3	32	STE	STE	None,exact	STE	IntelFP,exact	StableSPAM	False	TiesToEven	True	ignore	1.500	-0.043	to_one
llama_1B	Pure FP4	6.820	6.802	ESM3	32	STE	STE	None,exact	STE	None,exact	Adam	Fals	TiesToEven	False	N/A	0.000	-0.059	to_one
llama_1B	Pure FP4	2.269	2.375	N/A	N/A	N/A	N/A	N/A	N/A	Adam	Fals	N/A	N/A	N/A	N/A	N/A	N/A	N/A
llama_1B	Baseline	2.258	2.363	N/A	N/A	N/A	N/A	N/A	N/A	StableSPAM	False	N/A	N/A	N/A	N/A	N/A	N/A	N/A
llama_1B	Best Score (Neg)	2.322	2.437	ESM3	32	STE	STE	None,exact	STE	IntelFP,exact	StableSPAM	False	TiesToEven	True	ignore	1.500	-0.043	to_one
llama_1B	Best Score (Pos)	2.322	2.437	ESM3	32	STE	STE	None,exact	STE	IntelFP,exact	StableSPAM	False	TiesToEven	True	ignore	1.500	-0.043	to_one
llama_1B	Pure FP4	2.684	4.963	ESM3	32	STE	STE	None,exact	STE	None,exact	Adam	Fals	TiesToEven	False	N/A	0.000	-1.163	to_one
llama_60M	Baseline	2.665	2.657	N/A	N/A	N/A	N/A	N/A	N/A	StableSPAM	False	N/A	N/A	N/A	N/A	N/A	N/A	N/A
llama_60M	Baseline	2.983	3.028	N/A	N/A	N/A	N/A	N/A	N/A	StableSPAM	False	N/A	N/A	N/A	N/A	N/A	N/A	N/A
llama_60M	Best Score (Neg)	2.791	2.788	ESM3	32	STE	STE	None,exact	STE	IntelFP,exact	StableSPAM	False	TiesToEven	True	ignore	1.500	-0.071	to_one
llama_60M	Best Score (Pos)	2.791	2.788	ESM3	32	STE	STE	None,exact	STE	IntelFP,exact	StableSPAM	False	TiesToEven	True	ignore	1.500	-0.071	to_one
llama_60M	Pure FP4	5.056	5.050	ESM3	32	STE	STE	None,exact	STE	None,exact	Adam	Fals	TiesToEven	False	N/A	0.000	-0.897	to_one
llama_9M	Baseline	4.183	4.013	N/A	N/A	N/A	N/A	N/A	N/A	Adam	Fals	N/A	N/A	N/A	N/A	N/A	N/A	N/A
llama_9M	Baseline	4.141	3.972	N/A	N/A	N/A	N/A	N/A	N/A	StableSPAM	False	N/A	N/A	N/A	N/A	N/A	N/A	N/A
llama_9M	Best Score (Neg)	4.200	4.113	ESM3	32	STE	STE	None,exact	STE	IntelFP,exact	StableSPAM	False	TiesToEven	True	ignore	2.000	0.067	to_one
llama_9M	Best Score (Pos)	4.200	4.113	ESM3	32	STE	STE	None,exact	STE	IntelFP,exact	StableSPAM	False	TiesToEven	False	N/A	0.000	-0.313	to_one
llama_9M	Pure FP4	5.437	5.332	ESM3	32	STE	STE	None,exact	STE	None,exact	Adam	Fals	N/A	N/A	N/A	N/A	N/A	N/A
small_diffusion	Baseline	0.029	0.029	N/A	N/A	N/A	N/A	N/A	N/A	StableSPAM	False	N/A	N/A	N/A	N/A	N/A	N/A	N/A
small_diffusion	Baseline	0.019	0.019	N/A	N/A	N/A	N/A	N/A	N/A	StableSPAM	False	N/A	N/A	N/A	N/A	N/A	N/A	N/A
small_diffusion	Best Score (Neg)	0.018	0.019	ESM3	32	STE	STE	None,exact	STE	IntelFP,exact	StableSPAM	False	TiesToEven	False	N/A	1.000	0.027	to_one
small_diffusion	Best loss ESM3	0.018	0.019	ESM3	32	STE	STE	None,exact	STE	IntelFP,exact	StableSPAM	True	TiesToEven	False	N/A	1.500	0.021	nearest_subnormal
small_diffusion	Pure FP4	0.023	0.024	ESM3	32	STE	STE	None,exact	STE	None,exact	Adam	Fals	TiesToEven	False	N/A	0.000	-0.233	to_one

Figure 8: Training and validation performance curves for selected models and datasets of UE5M3 experiments.

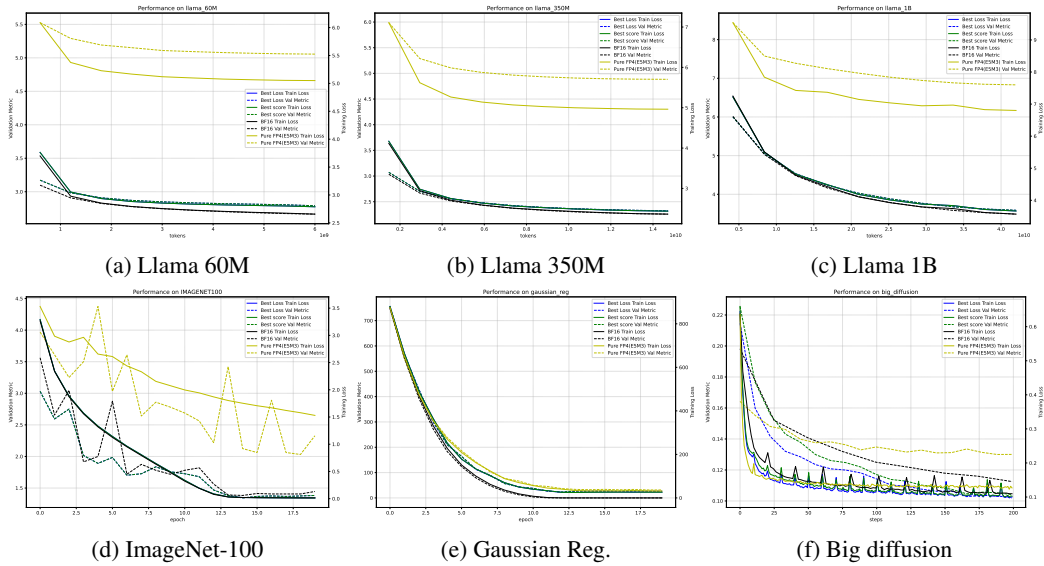


Figure 9: Training and validation performance curves for additional dataset for the UE5M3 scale

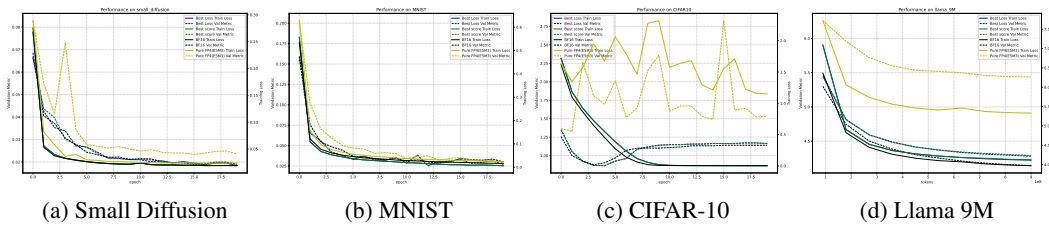
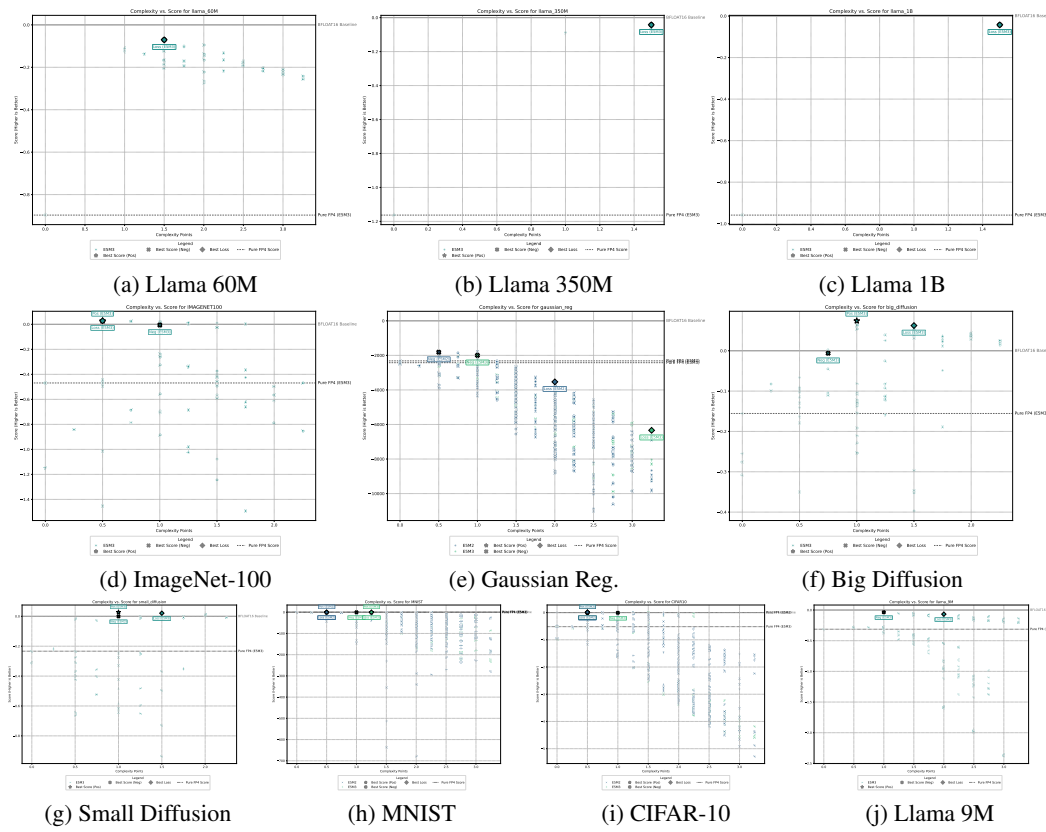


Figure 10: Pareto-frontier plots for each dataset, UE5M3 results. Note that we swept a smaller space compared to the main experiments.



.6 EXPERIMENTATION DETAILS

Complexity Score Calculation The complexity penalty $\Omega(c)$ is calculated based on the set of techniques \mathcal{T} used in a configuration. The total set of techniques and their corresponding weights w_t are detailed in Table 9. A configuration’s total complexity is the sum of weights for all techniques it employs, i.e., $\Omega(c) = \sum_{t \in \mathcal{T}_c} w_t$, where $\mathcal{T}_c \subseteq \mathcal{T}$.

Table 9: Complexity weights for non-baseline techniques.

Technique (t)	Activation Condition	Weight (w_t)
Non-STE Smoothing	smooth \neq 'STE'	3.0
Tensor Scaling Gradient Est.	tensor_scaling_grad_est is active	3.0
Non-STE Step Gradient	stepGradient \neq 'STE'	2.0
Hadamard Transform	use_hadamard is active	1.0
Non-STE Quantized Gradient	qGradient \neq 'STE'	1.5
Stochastic Rounding (SR)	SR is active	0.5
Tensor Scaling	use_tensor_scaling is active	0.5
Loss Scaling	loss_scaling is True	0.5
SPAM Optimizer	'SPAM' in optimiser name	0.5
Stochastic Rounding for scale	Scale rounding is Stochastic	0.25

We motivate the weight with reference to the added complexity and memory overhead, and fusability on a lower level language based on Table 2.

Table 10: Summary of the Full Hyperparameter Sweep.

Group	Parameter	Search Values
Quant.	Scale Format	{E8M0, E4M3}
	Max Approx.	{STE, softmax, hardsoftmax, absmax}
	Scale Rounding	{TiesToEven, TowardPositive, SR}
Gradient	Step Gradient	{STE, baseline, spline}
	Scaling Quant. ¹	{STE, baseline, spline}
	Tensor Scale Grad. ²	{ignore, absmax, STE}
Opt.	Optimizer	{Adam, StableSPAM}
	Loss Scaling	{True, False}
	Tensor Scaling	{True, False}
	SR	{None, all act., backward act.}
	Hadamard	{None, all, backward}

¹**Conditional:** Options for Scaling Quant. depend on the values of Max Approx.

²**Conditional:** Options for Tensor Scale Grad. depend on the values of Tensor Scaling and Max Approx.

Parameter sweeps

Dataset descriptions

Table 11: Summary of Experimental Setups

Learning Task	Dataset / Model	Global Batch Size	Seq. Length	Grad. Accum.	Learning Rate	Training Duration
Regression	Synthetic Gaussian	4096	-	-	1×10^{-2}	20 Epochs
Classification	MNIST	512	-	-	1×10^{-3}	20 Epochs
Classification	CIFAR-10	512	-	-	1×10^{-3}	20 Epochs
Classification	ImageNet-100	512	-	-	1×10^{-3}	20 Epochs
Image Generation	CIFAR-10 (Small U-Net, small_diffusion)	512	-	-	1×10^{-3}	20 Epochs
Image Generation	FFHQ (Big U-Net, big_diffusion)	20	-	-	1×10^{-4}	3 Epochs
Language Modeling	LLaMA-9M	4096	128	1	1×10^{-3}	0.9B Tokens [*]
Language Modeling	LLaMA-60M	128	512	1	1×10^{-4}	6B Tokens [*]
Language Modeling	LLaMA-350M	16	1024	8	1×10^{-4}	14.7B Tokens [*]
Language Modeling	LLaMA-1B	4	1024	512	1×10^{-4}	42B Tokens [*]

^{*}We use the WikiText dataset. Training duration is calculated based on parameter count (100x for models $< 350M$, $\approx 42 \times$ otherwise). We chose the token count based on Fishman et al. (2025), which show that training divergence in low precision usually happen around this amount of tokens relative to model size. Gradient accumulation is used for the 350M and 1B models. The 350M and 1B model configurations where taken directly from Tseng et al. (2025).

.7 DERIVATION OF PROPOSITION 1

The function for a single element is:

$$f_{ij} = \frac{1}{s_q} Q(s_q \mathbf{X}_{ij})$$

Since s_q is a function of \mathbf{X}_{ij} , we must use the product rule on: $\left(\frac{1}{s_q}\right)$ and $(Q(s_q \cdot \mathbf{X}_{ij}))$.

$$\frac{\partial f_{ij}}{\partial \mathbf{X}_{ij}} = \left(\frac{\partial}{\partial \mathbf{X}_{ij}} \frac{1}{s_q} \right) \cdot Q(s_q \mathbf{X}_{ij}) + \frac{1}{s_q} \cdot \left(\frac{\partial}{\partial \mathbf{X}_{ij}} Q(s_q \mathbf{X}_{ij}) \right)$$

Term 1: Derivative of $\frac{1}{s_q}$ This derivative depends on how s_q is defined by \mathbf{X} . Let $s = s(\mathbf{X})$.

$$\frac{\partial}{\partial \mathbf{X}_{ij}} \left(\frac{1}{s_q} \right) = -\frac{1}{s_q^2} \frac{\partial s_q}{\partial \mathbf{X}_{ij}} = -\frac{q'(s)}{s_q^2} \frac{\partial s}{\partial \mathbf{X}_{ij}}$$

Term 2: Derivative of $Q(s_q \mathbf{X}_{ij})$ We apply the chain rule to Q , and then the product rule to its argument $(s_q \mathbf{X}_{ij})$.

$$\begin{aligned} \frac{\partial}{\partial \mathbf{X}_{ij}} Q(s_q \mathbf{X}_{ij}) &= Q'(s_q \mathbf{X}_{ij}) \cdot \frac{\partial(s_q \mathbf{X}_{ij})}{\partial \mathbf{X}_{ij}} \\ \frac{\partial(s_q \mathbf{X}_{ij})}{\partial \mathbf{X}_{ij}} &= \left(\frac{\partial s_q}{\partial \mathbf{X}_{ij}} \right) \mathbf{X}_{ij} + s_q \left(\frac{\partial \mathbf{X}_{ij}}{\partial \mathbf{X}_{ij}} \right) = \mathbf{X}_{ij} \frac{\partial s_q}{\partial \mathbf{X}_{ij}} + s_q = \mathbf{X}_{ij} q'(s) \frac{\partial s}{\partial \mathbf{X}_{ij}} + s_q \end{aligned}$$

Thus, the full derivative of the second term is:

$$\frac{\partial}{\partial \mathbf{X}_{ij}} Q(s_q \mathbf{X}_{ij}) = Q'(s_q \mathbf{X}_{ij}) \left(\mathbf{X}_{ij} q'(s) \frac{\partial s}{\partial \mathbf{X}_{ij}} + s_q \right)$$

Combining and Final Result We substitute the results for both terms back into the main equation:

$$\frac{\partial f_{ij}}{\partial \mathbf{X}_{ij}} = \left(-\frac{q'(s)}{s_q^2} \frac{\partial s}{\partial \mathbf{X}_{ij}} \right) Q(s_q \mathbf{X}_{ij}) + \frac{1}{s_q} \left[Q'(s_q \mathbf{X}_{ij}) \left(\mathbf{X}_{ij} q'(s) \frac{\partial s}{\partial \mathbf{X}_{ij}} + s_q \right) \right]$$

Distributing the $\frac{1}{s_q}$ term:

$$\frac{\partial f_{ij}}{\partial \mathbf{X}_{ij}} = -\frac{q'(s)}{s_q^2} Q(s_q \mathbf{X}_{ij}) \frac{\partial s}{\partial \mathbf{X}_{ij}} + \frac{\mathbf{X}_{ij}}{s_q} Q'(s_q \mathbf{X}_{ij}) q'(s) \frac{\partial s}{\partial \mathbf{X}_{ij}} + \frac{s_q}{s_q} Q'(s_q \mathbf{X}_{ij})$$

Grouping the terms by their derivative component gives the final result for this fully general model:

$$\frac{\partial f_{ij}}{\partial \mathbf{X}_{ij}} = Q'(s_q \mathbf{X}_{ij}) + \frac{\partial s}{\partial \mathbf{X}_{ij}} \left[\frac{q'(s)}{s_q} \left(\mathbf{X}_{ij} Q'(s_q \mathbf{X}_{ij}) - \frac{1}{s_q} Q(s_q \mathbf{X}_{ij}) \right) \right] \quad (6)$$

.8 THEOREM 2 DERIVATION

Proof. We want to find the partial derivative of $h_{ij}(\mathbf{X})$ with respect to an element \mathbf{X}_{ij} . The transformation is defined as:

$$h_{ij}(\mathbf{X}) = g(\mathbf{X}) \cdot f_{ij}(\mathbf{U}_p)$$

where $g(\mathbf{X}) = \text{absmax}(\mathbf{X})$ and $\mathbf{U}_p = \mathbf{X}_p/g(\mathbf{X})$. An element \mathbf{X}_{ij} belongs to a specific block p .

1. **Apply the Product Rule.** We treat g and f_{ij} as two functions of \mathbf{X} . The product rule states $(uv)' = u'v + uv'$.

$$\frac{\partial h_{ij}}{\partial \mathbf{X}_{ij}} = \frac{\partial g}{\partial \mathbf{X}_{ij}} \cdot f_{ij}(\mathbf{U}_p) + g \cdot \frac{\partial f_{ij}(\mathbf{U}_p)}{\partial \mathbf{X}_{ij}}$$

2. **Apply the Chain Rule.** The second term's derivative requires the chain rule because f_{ij} is a function of $\mathbf{U}_{p,ij}$, which is a function of \mathbf{X}_{ij} .

$$\frac{\partial f_{ij}(\mathbf{U}_p)}{\partial \mathbf{X}_{ij}} = \frac{\partial f_{ij}}{\partial \mathbf{U}_{p,ij}} \cdot \frac{\partial \mathbf{U}_{p,ij}}{\partial \mathbf{X}_{ij}}$$

3. **Apply the Quotient Rule.** We find the derivative of $\mathbf{U}_{p,ij} = \mathbf{X}_{ij}/g$ with respect to \mathbf{X}_{ij} using the quotient rule $(\frac{u}{v})' = \frac{u'v - uv'}{v^2}$.

$$\frac{\partial \mathbf{U}_{p,ij}}{\partial \mathbf{X}_{ij}} = \frac{1 \cdot g - \mathbf{X}_{ij} \cdot \frac{\partial g}{\partial \mathbf{X}_{ij}}}{g^2} = \frac{1}{g} - \frac{\mathbf{X}_{ij}}{g^2} \frac{\partial g}{\partial \mathbf{X}_{ij}}$$

4. **Substitute and Combine.** Now, substitute the result from step (3) into step (2), and then the result of that into step (1).

$$\frac{\partial h_{ij}}{\partial \mathbf{X}_{ij}} = \frac{\partial g}{\partial \mathbf{X}_{ij}} f_{ij}(\mathbf{U}_p) + g \cdot \left[\frac{\partial f_{ij}}{\partial \mathbf{U}_{p,ij}} \left(\frac{1}{g} - \frac{\mathbf{X}_{ij}}{g^2} \frac{\partial g}{\partial \mathbf{X}_{ij}} \right) \right]$$

5. **Simplify and Rearrange.** Distribute the outer g into the brackets.

$$\frac{\partial h_{ij}}{\partial \mathbf{X}_{ij}} = \frac{\partial g}{\partial \mathbf{X}_{ij}} f_{ij}(\mathbf{U}_p) + \frac{g}{g} \frac{\partial f_{ij}}{\partial \mathbf{U}_{p,ij}} - \frac{g \cdot \mathbf{X}_{ij}}{g^2} \frac{\partial f_{ij}}{\partial \mathbf{U}_{p,ij}} \frac{\partial g}{\partial \mathbf{X}_{ij}}$$

The terms simplify, and we can replace $\frac{\mathbf{X}_{ij}}{g}$ with its definition, $\mathbf{U}_{p,ij}$.

$$\frac{\partial h_{ij}}{\partial \mathbf{X}_{ij}} = \frac{\partial g}{\partial \mathbf{X}_{ij}} f_{ij}(\mathbf{U}_p) + \frac{\partial f_{ij}}{\partial \mathbf{U}_{p,ij}} - \mathbf{U}_{p,ij} \frac{\partial f_{ij}}{\partial \mathbf{U}_{p,ij}} \frac{\partial g}{\partial \mathbf{X}_{ij}}$$

Finally, we group the terms containing $\frac{\partial g}{\partial \mathbf{X}_{ij}}$ to arrive at the theorem's statement.

$$\frac{\partial h_{ij}}{\partial \mathbf{X}_{ij}} = \frac{\partial f_{ij}}{\partial \mathbf{U}_{p,ij}} + \frac{\partial g}{\partial \mathbf{X}_{ij}} \left(f_{ij}(\mathbf{U}_p) - \mathbf{U}_{p,ij} \frac{\partial f_{ij}}{\partial \mathbf{U}_{p,ij}} \right)$$

This completes the proof. \square

.9 PROPOSITION 1 PROOF

Proof. The result follows directly from applying the chain rule to $s(Z(\mathbf{X}))$.

$$\frac{\partial s}{\partial \mathbf{X}_{ij}} = \frac{ds}{dZ} \cdot \frac{\partial Z}{\partial \mathbf{X}_{ij}} = \frac{d}{dZ} \left(\frac{\text{FP4 max}}{Z} \right) \frac{\partial Z}{\partial \mathbf{X}_{ij}} = -\frac{\text{FP4 max}}{Z(\mathbf{X})^2} \frac{\partial Z}{\partial \mathbf{X}_{ij}}$$

\square

.10 ABSMAX GRADIENT DERIVATION

Proof. Let (i^*, j^*) be the index of the element with the maximum absolute value, such that $Z(\mathbf{X}) = |\mathbf{X}_{i^*j^*}|$. We first find the gradient of $Z(\mathbf{X})$. The derivative of the absolute value function is the sign function, $\frac{d|x|}{dx} = \text{sign}(x)$. The derivative is non-zero only when we differentiate with respect to the element $\mathbf{X}_{i^*j^*}$ itself. This can be expressed precisely using the Kronecker delta:

$$\frac{\partial Z}{\partial \mathbf{X}_{ij}} = \frac{\partial |\mathbf{X}_{i^*j^*}|}{\partial \mathbf{X}_{ij}} = \text{sign}(\mathbf{X}_{i^*j^*}) \cdot \delta_{ii^*} \delta_{jj^*}$$

Substituting this result into the formula from Theorem 2 completes the proof.

$$\frac{\partial s}{\partial \mathbf{X}_{ij}} = -\frac{\text{FP4 max}}{Z(\mathbf{X})^2} \frac{\partial Z}{\partial \mathbf{X}_{ij}} = -\frac{\text{FP4 max}}{Z(\mathbf{X})^2} (\text{sign}(\mathbf{X}_{i^*j^*}) \cdot \delta_{ii^*} \delta_{jj^*})$$

\square

.11 SOFTMAX GRADIENT DERIVATION

Proof. We first find the gradient of $Z(\mathbf{X})$ by applying the chain rule multiple times.

$$\begin{aligned}
\frac{\partial Z}{\partial \mathbf{X}_{ij}} &= \frac{\partial}{\partial \mathbf{X}_{ij}} \left[\frac{1}{\beta} \log \left(\sum_{k,l} e^{\beta|\mathbf{X}_{kl}|} \right) \right] \\
&= \frac{1}{\beta} \cdot \frac{1}{\sum_{k,l} e^{\beta|\mathbf{X}_{kl}|}} \cdot \frac{\partial}{\partial \mathbf{X}_{ij}} \left(e^{\beta|\mathbf{X}_{ij}|} \right) \\
&= \frac{1}{\beta} \cdot \frac{1}{\sum_{k,l} e^{\beta|\mathbf{X}_{kl}|}} \cdot \left(e^{\beta|\mathbf{X}_{ij}|} \cdot \beta \cdot \text{sign}(\mathbf{X}_{ij}) \right) \\
&= \frac{e^{\beta|\mathbf{X}_{ij}|}}{\sum_{k,l} e^{\beta|\mathbf{X}_{kl}|}} \cdot \text{sign}(\mathbf{X}_{ij})
\end{aligned}$$

The fractional term is the definition of the softmax function applied to the scaled, absolute values of the tensor elements. Thus:

$$\frac{\partial Z}{\partial \mathbf{X}_{ij}} = \text{softmax}(\beta|\mathbf{X}|)_{ij} \cdot \text{sign}(\mathbf{X}_{ij})$$

Substituting this dense gradient back into the formula from Theorem 2 completes the proof. \square

$$\frac{\partial s}{\partial \mathbf{X}_{ij}} = -\frac{\text{FP4}}{Z(\mathbf{X})^2} \max \frac{\partial Z}{\partial \mathbf{X}_{ij}} = -\frac{\text{FP4}}{Z(\mathbf{X})^2} (\text{softmax}(\beta|\mathbf{X}|)_{ij} \cdot \text{sign}(\mathbf{X}_{ij}))$$

.12 TENSOR RECONSTRUCTION ERROR WITH MXFP4 FORMAT

Reconstruction error We first consider the reconstruction error, i.e., $|\mathbf{X} - \frac{1}{s_q} Q(s_q \cdot \mathbf{X})|$ for different choices of k , rounding modes of s , block sizes, and max functions $Z(\mathbf{X})$. We illustrate different slices of the relative error $\frac{|\mathbf{X} - \frac{1}{s_q} Q(s_q \cdot \mathbf{X})|}{|\mathbf{X}|}$. Figure 11 shows the reconstruction error for the Straight-Through Estimator (STE) as a function of block size. As expected, the error decreases as the block size increases.

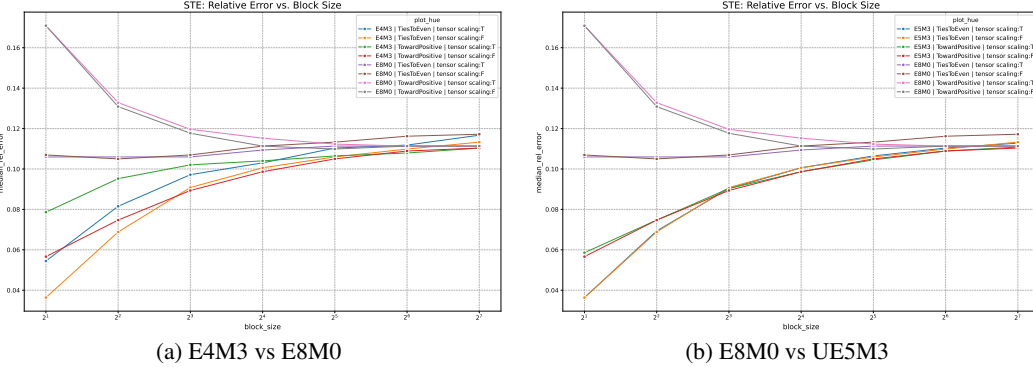


Figure 11: Reconstruction error using STE as a function of block size.

Experiment 2: STE Error vs. Tensor Scale Figure 12 illustrates the impact of the input tensor's scale on the STE reconstruction error, plotted on a log-log scale. These plots show comparisons for a fixed block size of 16.

Experiment 3: Softmax Error vs. Block Size Similar to the first experiment, Figure 13 shows the reconstruction error for the Softmax approximation as a function of block size, comparing different data formats.

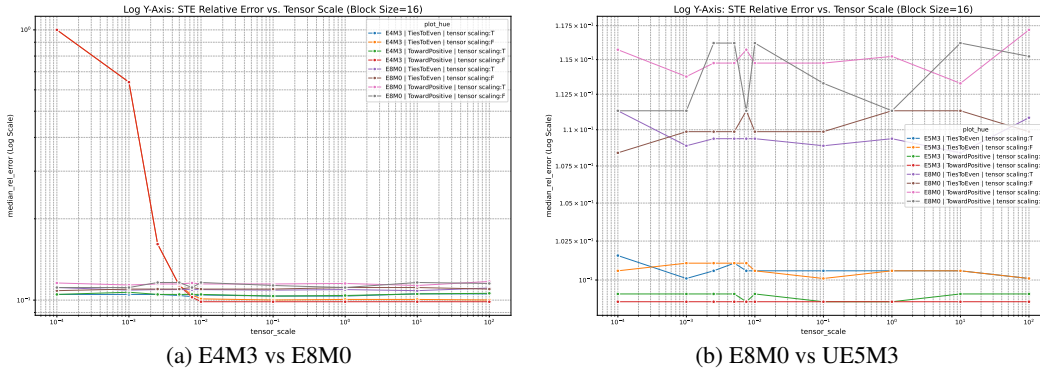


Figure 12: Reconstruction error using STE as a function of tensor scale (Block Size = 16).

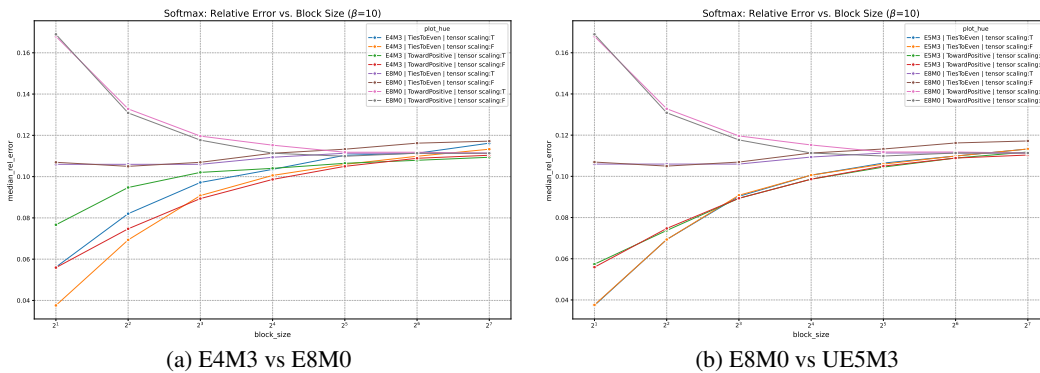


Figure 13: Reconstruction error using Softmax approximation as a function of block size.

Experiment 4: Softmax Error vs. Tensor Scale Figure 14 shows the effect of tensor scale on the Softmax approximation for a fixed block size of 16 and a β value of 40.

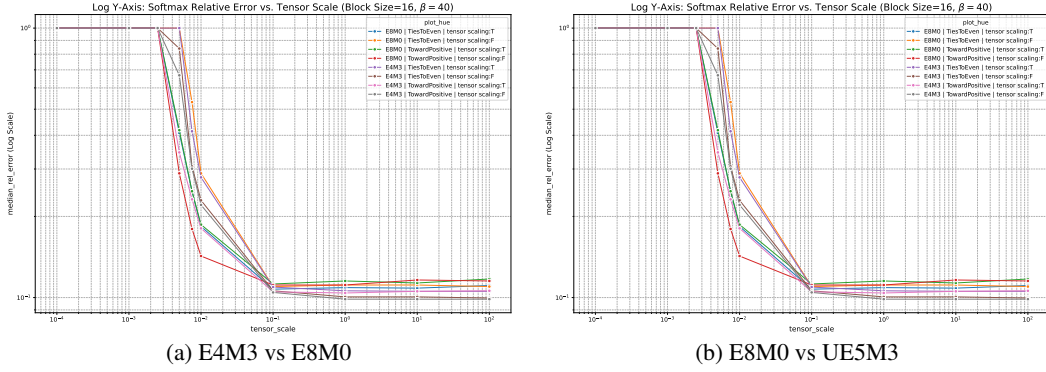


Figure 14: Reconstruction error using Softmax approximation as a function of tensor scale (Block Size = 16, β = 40).

Experiment 5: Softmax Sensitivity to β Finally, Figure 15 analyzes the sensitivity of the Softmax approximation to the inverse temperature parameter, β . The comparison highlights how tuning β affects the reconstruction error for different formats.

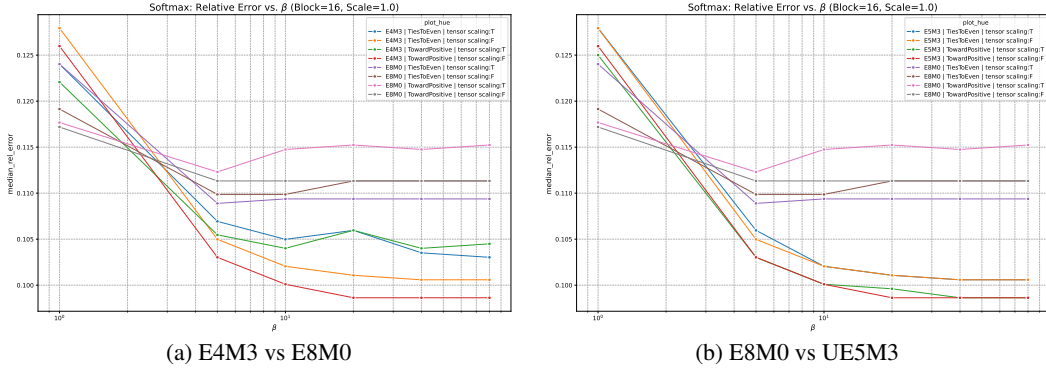


Figure 15: Reconstruction error using Softmax approximation as a function of the β parameter.

.13 THINGS WE TRIED BUT DIDN'T WORK

Conditional Block-wise Scaling As scaling factors have limited range, we found in our initial experiments that the E4M3 format tends to stall during training, which is caused by underflow due to its limited range compared to E8M0. We propose a conditional scaling strategy, where the choice is determined by comparing the dynamic range of the data's scales, $DR_{data} = \frac{g}{\tilde{g}}$, with the intrinsic dynamic range of the target scale format, $DR_{format} = \frac{E4M3_{max}}{E4M3_{min}}$. Here, $g = \max_p \{m_p\}$ and $\tilde{g} = \min_p \{m_p\}$.

Case 1: $DR_{data} \leq DR_{format}$ (Ideal Multiplicative Scaling) If the data's dynamic range fits within the format's range, we can compute a single constant C using the geometric mean to center the scales within the target range:

$$C = \frac{\sqrt{E4M3_{max} \cdot \tilde{g} \cdot E4M3_{min} \cdot g}}{FP4_{max}}$$

The full forward pass for an element, including the final de-normalization, is:

$$h_{ij}(\mathbf{X}) = \frac{C}{q(C \cdot s_p)} Q \left(\frac{q(C \cdot s_p)}{C} \cdot \mathbf{X}_{ij} \right)$$

where $q(\cdot)$ is the quantization function for the scales (e.g., rounding to the nearest E4M3 value).

Case 2: $\mathbf{DR}_{\text{data}} > \mathbf{DR}_{\text{format}}$ (Affine Mapping fallback) If the scaled dynamic range is too wide, we resort to using an affine transformation to map $s_p \in [\frac{\text{FP4}_{\max}}{g}, \frac{\text{FP4}_{\max}}{\tilde{g}}]$ to the range $[\text{E4M3}_{\min}, \text{E4M3}_{\max}]$. The affine parameters are:

$$a = \frac{\text{E4M3}_{\max} - \text{E4M3}_{\min}}{\frac{\text{FP4}_{\max}}{\tilde{g}} - \frac{\text{FP4}_{\max}}{g}}, \quad b = \text{E4M3}_{\max} - a \cdot \frac{\text{FP4}_{\max}}{\tilde{g}}$$

The scale to be quantized is $\tilde{s}_p = a \cdot s_p + b$. We can then combine this with tensor scaling to achieve a reasonable quantisation:

$$h_{ij}(\mathbf{X}) = \frac{g \cdot \text{E4M3}_{\max}}{\text{FP4}_{\max} \cdot q(\tilde{s}_p)} Q \left(q(\tilde{s}_p) \cdot \frac{\mathbf{X}_{ij} \cdot \text{FP4}_{\max}}{g \cdot \text{E4M3}_{\max}} \right)$$

In the above setting, we're mapping the scale s_p to the full range of E4M3, however due to the affine mapping we may lose precision for cases when $m_p \ll g$, since the term $\frac{\mathbf{X}_{ij} \cdot \text{FP4}_{\max}}{g \cdot \text{E4M3}_{\max}}$ will not have the full FP4_{\max} range. We motivate this trade-off with the observation that NVFP4 has a block-size of 16, implying that having a well-represented scale outweighs the block accuracy.

When we tested the above on CIFAR10 as a unit test for E4M3 we couldn't get anywhere near convergence.

Sigmoid approximation Let $\mathcal{V} = \{v_1, \dots, v_n\}$ denote FP4 (E2M1) levels. Define intervals $I_i = (v_i, v_{i+1}]$, $i = 1, \dots, n-1$, with

$$c_i = \frac{v_i + v_{i+1}}{2}, \quad \Delta_i = v_{i+1} - v_i, \quad \gamma_i = \frac{12}{\Delta_i}.$$

For $x \in I_i$, let

$$z_i(x) = \frac{(x - c_i)\gamma_i}{T}, \quad w(x) = \sigma(z_i(x)) = \frac{1}{1 + e^{-z_i(x)}}.$$

Proposition 3 (Smooth Quantization Properties). *Let $Q(x)$ be defined as above. Then:*

1. *The forward mapping $Q(x) = v_i + w(x)\Delta_i$ is a smooth interpolation between v_i and v_{i+1} using a sigmoid.*

2. *Its derivative is*

$$Q'(x) = \Delta_i \cdot \sigma(z_i)(1 - \sigma(z_i)) \cdot \frac{\gamma_i}{T} = \frac{12}{T} \sigma(z_i)(1 - \sigma(z_i)).$$

3. *In the limit $T \rightarrow 0$, $Q(x)$ converges to the standard ties-to-even quantization:*

$$\lim_{T \rightarrow 0} Q(x) = \begin{cases} v_i, & x \leq c_i \\ v_{i+1}, & x > c_i \end{cases}.$$

Proof. The forward mapping is linear in v_i and v_{i+1} with a weight $w(x) \in (0, 1)$ from the sigmoid, so it is smooth and bounded by v_i and v_{i+1} .

For the derivative:

$$Q'(x) = \frac{d}{dx} (v_i + w(x)\Delta_i) = \Delta_i \frac{dw}{dx} = \Delta_i \frac{dw}{dz_i} \frac{dz_i}{dx}.$$

Since $w = \sigma(z_i)$, we have $\frac{dw}{dz_i} = \sigma(z_i)(1 - \sigma(z_i))$, and $dz_i/dx = \gamma_i/T$, giving

$$Q'(x) = \Delta_i \cdot \sigma(z_i)(1 - \sigma(z_i)) \cdot \frac{\gamma_i}{T} = \frac{12}{T} \sigma(z_i)(1 - \sigma(z_i)).$$

Finally, as $T \rightarrow 0$, the sigmoid becomes a step function at c_i :

$$\sigma\left(\frac{(x - c_i)\gamma_i}{T}\right) \rightarrow \begin{cases} 0, & x < c_i \\ 1, & x > c_i \end{cases},$$

so $Q(x)$ reduces to ties-to-even quantization:

$$Q(x) \rightarrow \begin{cases} v_i, & x \leq c_i \\ v_{i+1}, & x > c_i \end{cases}.$$

□

We tried this gradient adjustment, we expected it would provide a significant performance benefit, however this was not the case in early experiments (MNIST, gaussian regression, CIFAR10, llama 9M). Hence on lower level implementations, the additional complexity is not justified. The additional complexity is $\mathcal{O}(np \log k)$, with $\mathcal{O}(n)$ extra memory. p denotes the number of polynomials used to evaluate the exponential function used in the sigmoid.